ABSTRACT

Title of Thesis: BASEBAND IMPLEMENTATION AND

PERFORMANCE ANALYSIS

OF THE MULTIBAND OFDM UWB SYSTEM

Hung-Quoc Duc Lai, Master of Science, 2006

Thesis directed by: Professor K. J. Ray Liu

Department of Electrical and Computer Engineering

In this thesis, we follow the standard proposal IEEE 802.12.3a to implement the MB-OFDM UWB system in C programming language. We also analyze the system performance in the multipath fading channel, the IEEE 802.15.3a channel standard. Four different conditions of frequency and timing synchronization are considered. Since the entire system consists of two subsystems: (a) the channel coding with the bit-interleaving and (b) OFDM modulation, the analysis is proceeded in two stages. First, we consider the performance of the only OFDM subsystem. Degradation ratio and average bit error probability are the two metrics used to evaluate the performance. Secondly, we provide the performance bound of the entire UWB system. The performance analysis provides a good understanding of the system behavior in the IEEE 802.15.3a channel standard under various synchronization

conditions. The knowledge about the performance of the MB-OFDM UWB system defines our main contribution to the area of wireless communications.

BASEBAND IMPLEMENTATION AND
PERFORMANCE ANALYSIS
OF THE MULTIBAND OFDM UWB SYSTEM

by

Hung-Quoc Duc Lai

Thesis submitted to the Faculty of the Graduate School of the
University of Maryland, College Park in partial fulfillment
of the requirements for the degree of
Master of Science
2006

Advisory Commmittee:

    Professor K. J. Ray Liu, Chair/Advisor
    Professor Steven Tretter
    Professor Min Wu

To my wife Lethy and my son Quoc-Viet

ACKNOWLEDGMENTS

I owe my gratitude to all the people who have made this thesis possible and because of whom my graduate experience has been one that I will cherish forever.

First and foremost, I would like to thank my advisor, Professor K. J. Ray Liu for giving me an invaluable opportunity to work on a challenging and extremely interesting project over the past year. He has always made himself available for help and advice. It has been a pleasure to work with and learn from such an extraordinary individual.

I would also like to thank Professor Steven Tretter and Professor Min Wu for agreeing to serve on my thesis examination committee and for sparing their invaluable time reviewing the manuscript.

Thanks are due to Dr. Wipawee (Pam) Siriwongpairat and Dr. André Kwasinski for devoting their time in helping me in this work. Their willingness is invaluable.

My colleagues in Signals and Information Group at the Communications and Signal Processing Laboratory, University of Maryland have enriched my graduate life in many ways and deserve a special mention. Specifically, Thanongsak (Kee) Himsoon and Steve Tjoa were always available for me to discuss about my thesis and helped

me writing this thesis in LaTex.

I would also like to thank Dorothea Brosius for providing the LaTex style files for writing this thesis.

I owe my deepest thanks to my mother and father who bore me to this life and brought me here for a better education and life. My deepest thanks are also given to my aunt who raised me through my difficult childhood and to my wife who has always stood by me, shared with me the fruits of life as well as its bitterness, and encouraged me in my work. Words cannot express the gratitude I owe them.

I would like to acknowledge the financial support from the Gates Millennium Scholars. Without that, it would be difficult for me to follow this program and complete this thesis.

It is impossible to remember all, and I apologize to those I have inadvertently left out.

Lastly, thank you all and thank God!

TABLE OF CONTENTS

LIST OF TABLES

LIST OF FIGURES

LISTS OF ACRONYMS AND ABBREVIATIONS

AWGN   Additive White Gaussian Noise
BER   Bit Error Rate
BPSK   Binary-Phase Shift Keying
CDMA   Code Division Multiple Access
CM   Channel Model
DS   Direct Sequence
DSSS   Direct-Sequence Spread Spectrum
EIRP   Effective Isotropically-Radiated Power
Eq.   Equation
Eqs.   Equations
FCC   Federal Communications Commission
FFT   Fast Fourier Transform
FH   Frequency Hopping
ICI   Inter-Carrier Interference
IFFT   Inverse Fast Fourier Transform
ISI   Inter-Symbol Interference
kbps   kilobits per second
LOS   Line-Of-Sight
MB   Multiband
Mbps   Megabits per second
MC   Multicarrier
MGF   Moment Generating Function
ML   Maximum Likelihood
NLOS   non-LOS
OFDM   Orthogonal Frequency Division Multiplexing
PDF   Probabilistic Density Function
PRBS   Pseudo Random Binary Sequence
QPSK   Quadrature-Phase Shift Keying
SNR   Signal-to-Noise Ratio
UWB   Ultra-WideBand
WPAN   Wireless Personal Area Network

Chapter 1

Introduction

1.1 The Emergence, the Potential and the Technical Approaches of the UWB Transmission Technology

In April 2002, the U.S. Federal Communications Commission (FCC) published a report and order "Revision of Part 15 of the Commission Rules Regarding to Ultra-Wideband Transmission Systems" [1] that allows Ultra-WideBand (UWB) communication systems to be deployed on an unlicensed basis following Part 15 rules. The publication encourages researchers and scientists to devote their time and resources to the development of the UWB transmission technology. According to the FCC's definition, a UWB device is any device where the fractional bandwidth is greater than 20% of its center frequency or the minimum bandwidth limit is 500 MHz. Besides, the FCC also defines the transmission power limits. Table 1.1 presents the UWB power limitation corresponding to different frequency ranges [1]. As a result, UWB devices are allowed to coexist with other existing devices such as devices using 802.11a. Figure 1.1 illustrates the UWB frequency allocation and the coexistence between UWB devices and others. Since the FCC's publication, researchers and scientists have focused their attention to the frequency range 3.1 GHz to 10.6 GHz with the transmission power limit of - 41.3 dBm/MHz. From the

table, the 3.1-to-10.6GHz frequency range is obviously the major part with highest transmission power allowance.

Frequency in MHZ	Effective isotropically-radiated power (EIRP) in dBm
Below 960	15.209 limits
960 - 1610	- 65.3
1610 - 1990	- 53.3
1990 - 3100	- 51.3
3100 - 10600	- 41.3
Above 10600	- 51.3

Table 1.1: **UWB transmission power limits.**
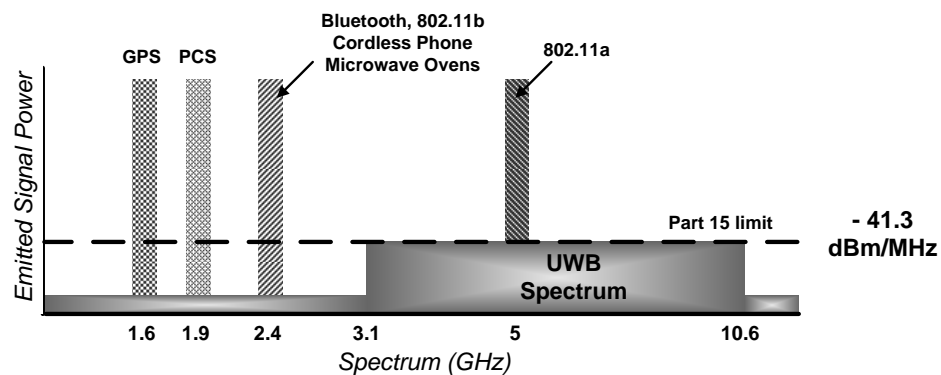
Figure 1.1: **UWB spectrum.**

To see the potential of the UWB transmission technology, it is worthy to look at the evolution of wireless transmission. Historically, human being has an enduring demand for high transmission data rates. People want to communicate any type of information with anyone, at anytime, from anywhere, and that is only possible with the support of wireless technology [2]. Wireless mobile communication systems

have been developed through several generations [2], [3], [4]. In the early 1980s, the first generation (1G) was emerged. The systems provided analog voice service and the transmission data rates was up to 2.4kbps. The development of the 1G was completed in the early of 1990s. The second generation (2G) was introduced in the late 1980s and completed in the late 1990s. In this generation, the wireless systems provided digital voice services with enhanced calling features like caller ID. The transmission data rates were up to 64kbps. The first two generations belong to the narrowband era. The third generation (3G) was developed in the late 1990s and is predicted to complete in the late of 2000s. This generation belongs to the wideband era. It is aimed to provide many services such as superior voice quality and data always add-on. The transmission data rates are from 125kbps to 2Mbps. While the development of the 3G is still going on, researchers begin looking forward to the fourth generation (4G) of wireless transmission, which belongs to the broadband era. This generation will provide multimedia services at a lower cost. The transmission data rates are expected at least 100Mbps.

The UWB transmission technology promises to fulfill the demand of high transmission data rates with a low cost and power consumption [5]. With its wide transmission bandwidth, UWB systems possess high transmission capacity since the channel capacity C (bits/s) of band-limited Gaussian channel is [6]

$$C = W \log_2 \left(1 + \frac{S}{N} \right) \tag{1.1}$$

where W is the channel bandwidth (Hz), S and N are the power (watts) of the signal and noise, respectively. Equation (1.1) reveals that the channel capacity

depends linearly to the channel bandwidth but only logarithmically to the signal-to-noise ratio (SNR), and thus the available bandwidth is more important than the power of the transmission. The larger in bandwidth of the systems is the higher in transmission capacity. As being shown, UWB transmission technology can provide transmission data rates up to 400Mbps [7] [8]. It fits into the high data rate wireless personal area network (WPAN) whose transmission distance is between 1 to 10 m [5]. The UWB transmission technology is predicted as one of components in the wireless transmission 4G [3] [5].
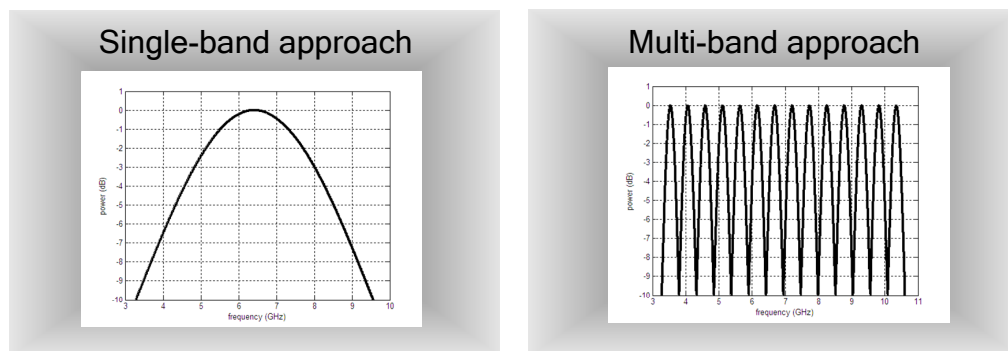
Figure 1.2: **UWB approaches (a) Single-band. (b) Multi-band.**

To exploit the unlicensed 7.5GHz bandwidth, two technical approaches mainly have been proposed. The first approach is the direct-sequence UWB (DS-UWB) relating to single-band systems. In this approach, the information is directly BPSK-modulated into a sequence of impulse-like waveform [7]. Each pulse has a very small duration of less than 1 nsec, and it occupies the entire available 7.5GHz bandwidth as illustrated in Figure 1.2(a). The second approach involves multiband (MB) systems, and thus called MB-UWB. Figure 1.2(b) demonstrates the multiband approach in

which the 7.5GHz bandwidth is divided into subbands of more than 500 MHz each to comply with the FCC's definition. The dominant candidate of the multiband approach is the MB-OFDM UWB [8], which employs Orthogonal Frequency Division Multiplexing (OFDM) technique. The DS-UWB and MB-OFDM UWB are trying to gain the support of the IEEE 802.15.3a committee to become the standard for the high speed WPAN standard [9].

1.2 Motivations

In Section 1.1, we have seen that UWB has a large potential in the near-future wireless transmission. It will be a core component in the coming 4G. Therefore, understanding the UWB transmission technology becomes important and is the main motivation for the work in this thesis. As presented in Section 1.1, there are two dominant approaches: DS-UWB and MB-OFDM UWB to the use of the unlicensed 7.5GHz bandwidth. The DS-UWB system is based on direct-sequence spread spectrum (DSSS) techniques [7], which are well understood and have been proven in other commercial technologies. However, dealing with the extremely wideband signal is a challenge. One of concerns in DS-UWB is its low ability to combat the inter-symbol interference (ISI) since the spreading factor is relatively small for high data rates. The MB-OFDM UWB system combines the frequency hopping (FH) and OFDM technique [8]. The use of OFDM strengthens the UWB system against the ISI due to multipath effects and eliminates the use of a complex equalizer.

In this thesis, we focus our attention on the MB-OFDM UWB system because

we believe that OFDM will be the main transmission technique in the future 4G. Implementation is important in helping us to understand the architecture of the system and that is one of the main parts of this thesis. In this thesis, we follows the MB-OFDM UWB standard proposal IEEE 802.15.3a [8] to implement the system in C programming language. In addition, studying the performance of the MB-OFDM UWB system in multipath fading channel, the IEEE 802.15.3a standard channel [10], is more important since the knowledge of the system performance would help us improving it. Thus obtaining the performance analysis of the MB-OFDM UWB system is our other main task in this thesis.

So far, no ones have completely analyzed the performance of the MB-OFDM UWB system in the IEEE 802.15.3a standard channel. In 2004, Park *et al.* compared the performance between DS-CDMA, OFDM, and MC-CDMA UWB in the multipath fading channel based on simulation [11]. In 2005, Shin *et al.* evaluated the performance of the MB-OFDM UWB and DS-UWB systems but also based on simulation [12]. In 2005, Snow *et al.* analyzed the performance of the MB-OFDM UWB system under the imperfection of channel estimation [13]. In 2005, Siriwong-pairat *et al.* provided a landmark for the performance analysis of the MB-OFDM UWB system in the IEEE 802.15.3a channel standard [14]. All of the work assumed perfect frequency and timing synchronization. In addition, they assumed that the channel multipath delays fit inside the cyclic prefix of the OFDM symbols, and hence the system does not suffer the ISI effect. In reality, the multipath channel delays, however, exceed the length of the cyclic prefix for all channel models in the IEEE channel standard and really cause the ISI to the received signal in the system.

Due to the incompletion of the previous work, we now analyze the performance of the MB-OFDM UWB system with considering this ISI effect. Furthermore, because OFDM transmission technique is sensitive to the frequency and timing synchronization, we would like to learn the system performance in different synchronization conditions. Particularly, we consider the following four synchronization scenarios:

1. Perfect frequency and timing synchronization,

2. Imperfect timing synchronization,

3. Imperfect frequency synchronization, and

4. Imperfect frequency and timing synchronization.

The system performance is measured by two metrics. The first metric is the degradation ratio that measures the degradation of the system performance. The second metric is the average bit error probability. In the next section, we will outline the content of this thesis.

1.3 Outline of Thesis

As we have seen, Chapter 1 introduces the emergence and the potential of the UWB transmission technology. In addition, it presents our motivations for the work in this thesis. We would really like to learn about the MB-OFDM UWB system since the MB-OFDM UWB is the future wireless transmission technology. In Chapter 2, we will describe the baseband implementation of the MB-OFDM UWB system. The implementation follows the MB-OFDM UWB standard proposal IEEE 802.15.3a in

a straightforward manner. Chapter 3, a very important chapter which defines our main contribution in this thesis, presents the performance analysis of the UWB system in IEEE 802.15.3a standard channel models. We will consider the system in the four frequency and timing synchronization scenarios presented in Section 1.2. As we will see, the MB-OFDM UWB system consists of two main blocks: the channel coding and the OFDM modulation. Thus system performance will be analyzed in two stages. First, we will analyze the performance of the OFDM system. The degradation ratio and the average bit error probability are the two metrics used to measure the system performance. We will provide the derivation of these metrics in the chapter. Secondly, the performance bound of the entire MB-OFDM UWB system will be provided based on the average bit error probability obtained in the first stage. Also in the chapter, we will present the numerical and simulated results. In the last chapter, Chapter 4, we conclude the work in this thesis and emphasize our main contribution to the area of wireless communication. Lastly, we will provide the C programming codes for the main function of the transmitter and receiver of the MB-OFDM UWB system in Appendix at the end of this thesis.

Chapter 2

Baseband Implementation of the MB-OFDM UWB System

2.1 Overview

The baseband implementation of the MB-OFDM UWB system follows the standard proposal IEEE 802.15.3a [8]. The entire unlicensed 7.5-GHz band is divided into fourteen subbands, as illustrated in Figure 2.1. The bandwidth of each subband
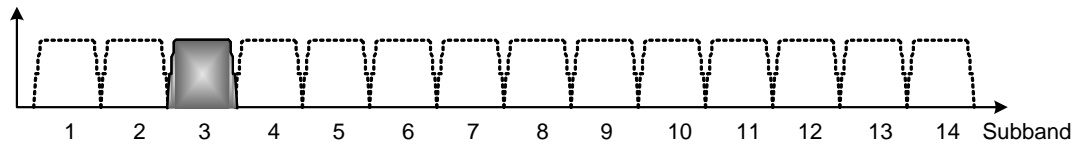
Figure 2.1: **Band division.**

is 528 MHz to satisfy the FCC's definition of UWB transmission. The UWB system employs OFDM with 128 sub-carriers. Quadrature Phase Shift Keying (QPSK) is used to modulate the transmit signal at the subcarriers. The reason for using QPSK is due to the limitation of the transmit power, which is not allowed to exceed - 41.3 dBm/MHz [1]. Each OFDM symbol is pre-appended with a cyclic prefix (actually a zero-trailing, i.e., filling the prefix by zeros) to eliminate the ISI. The guard interval is appended to the OFDM symbol to ensure the transition between the two consecutive symbols. The durations of the useful OFDM symbol, the cyclic prefix, and the guard interval are $T_S = 242.42$ nsec, $T_C = 60.61$ nsec, and $T_G = 9.47$ nsec. Figure 2.2 illustrates the OFDM transmission technique.

9
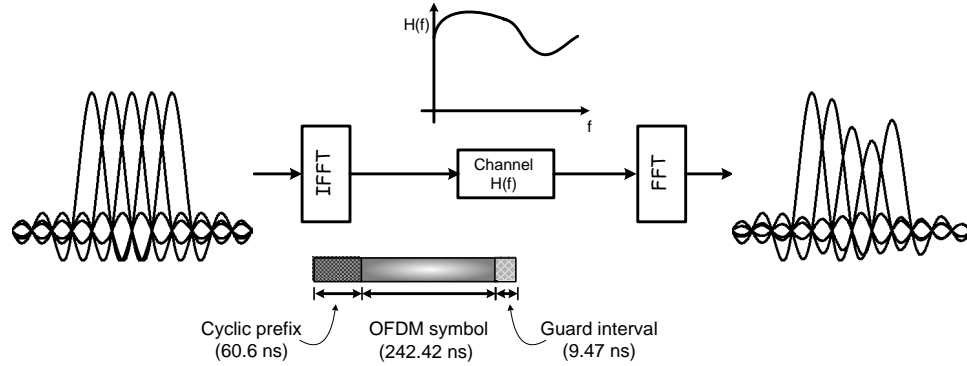
Figure 2.2: **OFDM transmission.**

Table 2.1 presents the data-rate dependent parameters for the MB-OFDM UWB system. The system supports ten different transmission data rates: 53.3, 55, 80, 106.7, 110, 160, 200, 320, 400, and 480 (Mbps). As we have mentioned, QPSK is used for the modulation of signals at the subcarriers. The system imposes five different coding rates: 1/3, 11/32, 1/2, 5/8, and 3/4. Depending on the data rates, we obtain different overall spreading gain: a factor of 4 for the first three data rates, a factor of 2 for the next four data rates, and a factor of 1 (no spreading gain) for the last three data rates.

Figure 2.3 illustrates the transmitter and the receiver of the MB-OFDM UWB system. They consist of two parts: baseband and radio frequency (RF). The baseband of the transmitter consists of a data scrambler, a convolutional encoder and puncturer, a bit-interleaver, a constellation mapper, and an inverse fast Fourier transform (IFFT). The baseband of the receiver, in general, consists of similar blocks of the baseband in the transmitter but in the reverse order. In the next sections, we will describe in detail the implementation of these blocks. The C programming codes for the transmitter and the receiver of the MB-OFDM UWB system will be

(a)

(b)
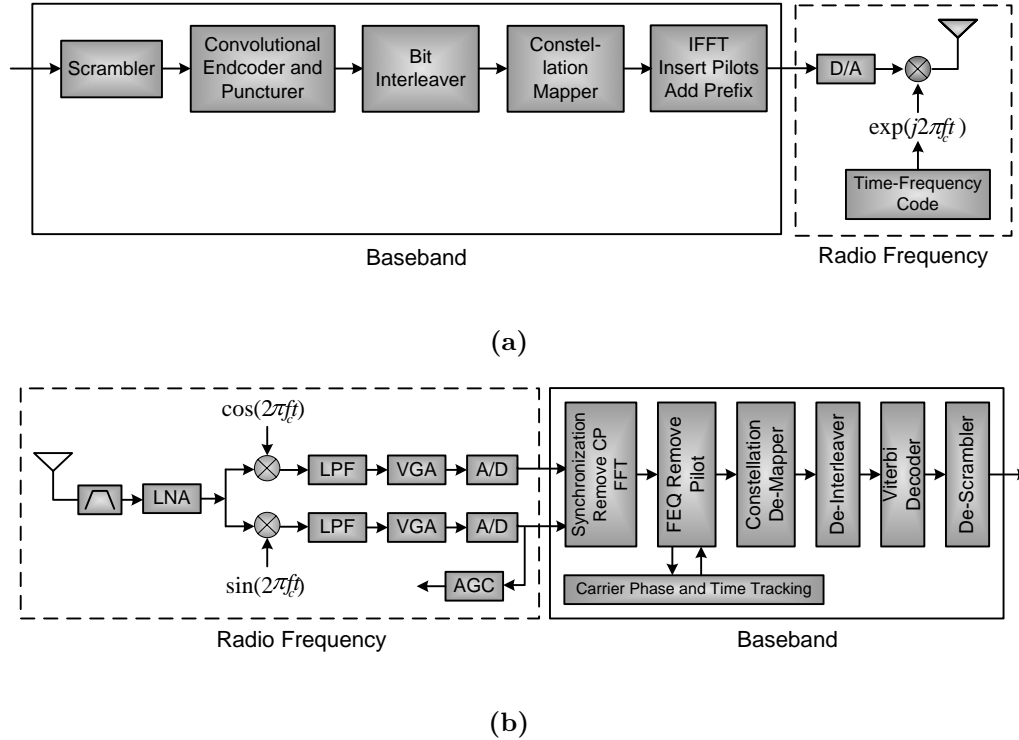
Figure 2.3: **UWB system (a) Transmitter; (b) Receiver.**

provided in Appendix at the end of this thesis.

2.2 Scrambler and De-scrambler

The first block in the baseband of the UWB transmitter is a data scrambler. The purpose of the data scrambler is to convert a data bit sequence into a pseudo random sequence that is free from long strings of simple patterns such as marks and spaces [15]. The polynomial generator of the pseudo random binary sequence (PRBS) is

$$g(D) = 1 + D^{14} + D^{15} \tag{2.1}$$

where D represents a single bit delay. The corresponding PRBS x_n is generated as

$$x_n = x_{n-14} \oplus x_{n-15} \tag{2.2}$$

11

Data rate (Mbps)	Modulation	Coding rate (R)	Frequency spreading factor	Time spreading factor	Overall spreading gain	Coded bits per OFDM symbol (N_{CBPS})
53.3	QPSK	1/3	Yes	2	4	100
55	QPSK	11/32	Yes	2	4	100
80	QPSK	1/2	Yes	2	4	100
106.7	QPSK	1/3	No	2	2	200
110	QPSK	11/32	No	2	2	200
160	QPSK	1/2	No	2	2	200
200	QPSK	5/8	No	2	2	200
320	QPSK	1/2	No	1	1	200
400	QPSK	5/8	No	1	1	200
480	QPSK	3/4	No	1	1	200

Table 2.1: **Data-rate dependent parameters.**

where "$\oplus$" represents modulo-2 addition. The scrambled data bitstream is obtained as

$$s_n = b_n \oplus x_n \tag{2.3}$$

where b_n is the unscrambled data bitstream.

The scrambler and de-scrambler are initialized with the same "seed-value", which is chosen based on the first two bits b_0 and b_1 in the unscrambled data sequence. They are called the "seed-identifiers". The correspondence between seed-values and seed-identifiers follows Table 2.2.

Seed identifier (b_1, b_0)	Seed value $(x_{14} \; ... \; x_0)$
0,0	0011 11111111 111
0,1	0111 11111111 111
1,0	1011 11111111 111
1,1	1111 11111111 111

Table 2.2: **Scrambler seed selection.**

2.3 Convolutional Encoder and Viterbi Decoder

The second block in the baseband of the UWB transmitter is the convolutional encoder and puncturer. This block serves to add patterns of redundancy to the data in order to improve the SNR for more accurate decoding at the receiver. The system supports five different coding rates: 1/3, 11/32, 1/2, 5/8, and 3/4. The code corresponding to coding rate 1/3 is called the mother code whose generator polynomials are $g_0 = [133_8]$, $g_1 = [145_8]$, and $g_2 = [175_8]$ and constraint length is $K = 7$. Figure 2.4 illustrates the mother convolutional encoder. An input data bit
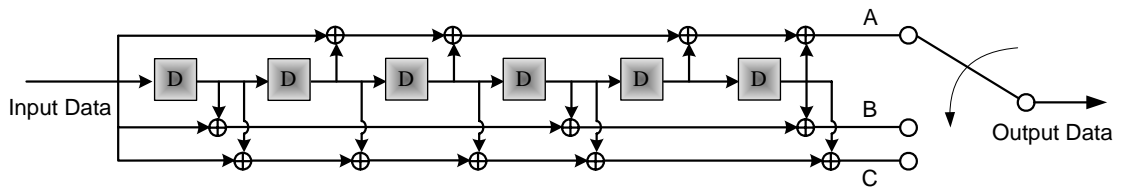
Figure 2.4: **Mother convolutional encoder.**

produces three output bits and thus yields the coding rate 1/3. These output bits are denoted as A, B, and C where A is the first bit, B is the second bit, and C is the last bit. They are formed in the order of ABC to yield the output sequence.

Figure 2.5 shows the input-output relation of the mother convolutional code. At the receiver, Viterbi decoder is employed to decode the convolutional encoded sequence.

X_0	X_1	X_2	X_3	X_4	X_5	X_6

$\Downarrow$

A_0	A_1	A_2	A_3	A_4	A_5	A_6
B_0	B_1	B_2	B_3	B_4	B_5	B_6
C_0	C_1	C_2	C_3	C_4	C_5	C_6
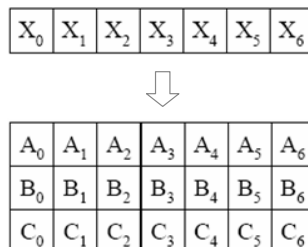
Figure 2.5: **Input-output relation of mother convolutional encoder.**

Other coding rates are obtained through puncturing the mother code. The puncturer simplifies the implementation since we need not to have other convolutional encoders for these coding rates. Puncturing is a procedure for omitting some encoded bits at the transmitter and inserting a dummy "zero" metric into the received sequence at the receiver in the place of the omitted bits. The inserted dummy "zero" metric should result in no change to the accumulated error in the decoding process [16]. Figure 2.6(a) describes how coding rate 11/32 can be obtained from the mother code. Eleven bits from x_0 to x_{10} are input to the encoder and result in thirty three output bits from A_0 to C_{10}. By omitting the bit C_{10}, we obtain the coding rate of 11/32, i.e., that eleven input bits produce thirty two output bits. At the receiver, we insert a dummy bit in the place C_{10} and then input the received sequence to a Viterbi decoder to obtain 11 decoded bits.

In a similar manner, we also obtain other coding rates. Figures 2.6(b), 2.6(c), and 2.6(d) show the puncturing patterns of the coding rates 1/2, 5/8, and 3/4,
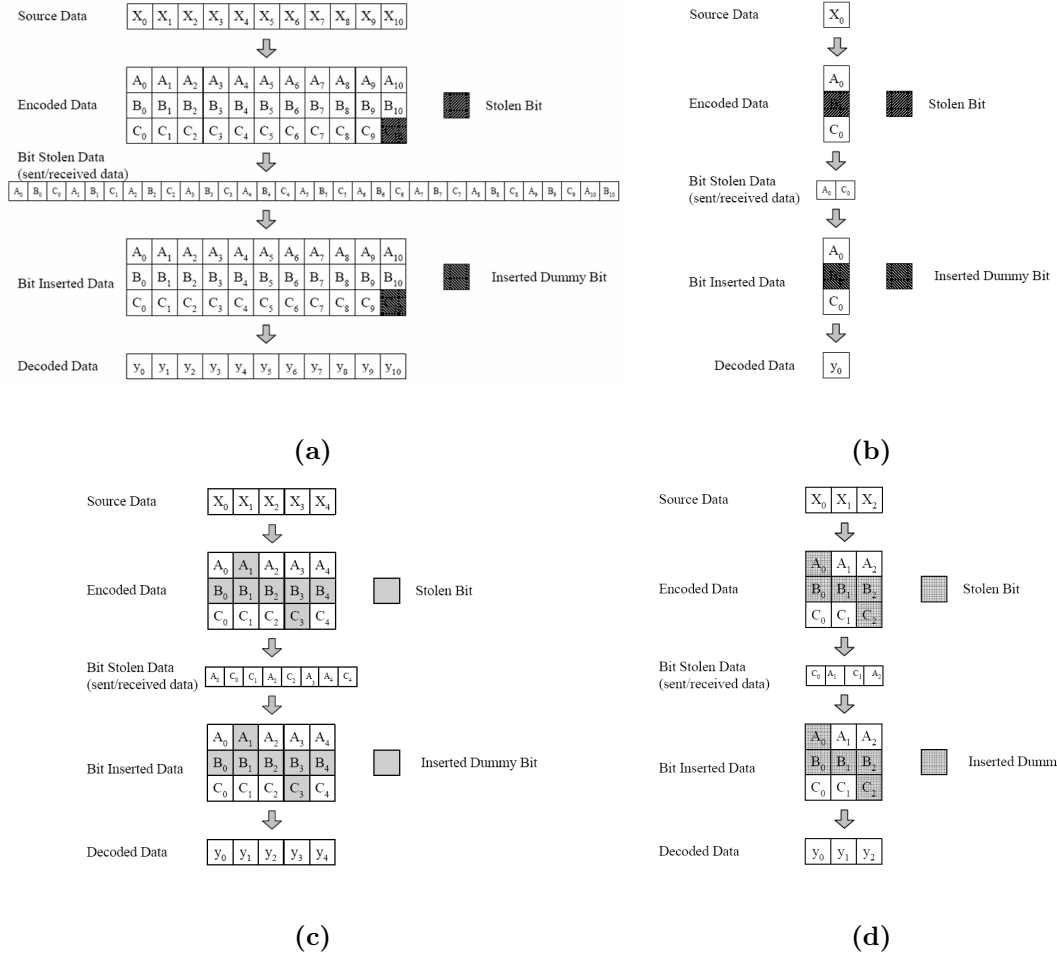
Figure 2.6: **Puncturing patterns (a) R = 11/32; (b) R = 1/2; (c) R = 5/8; (d) R = 3/4.**

respectively, and illustrate the puncturing process of these coding rates.

2.4 Bit Interleaver and De-interleaver

The third block in the baseband of the UWB transmitter is the bit interleaver. The purpose of the bit interleaver is to provide robustness against burst errors [17]. The bit interleaving operates through two stages, a symbol interleaving followed by a tone interleaving. In the symbol interleaving, the bits across 6 OFDM sym-

15

bols are permuted to exploit frequency diversity across the subbands. In the tone interleaving, the bits across data tones within an OFDM symbol are permuted to exploit frequency diversity across tones. The input-output relations in the symbol interleaving and tone interleaving are as follows.

$$
S(i) = U\left\{\mathbf{Floor}\left(\frac{i}{N_{CBPS}}\right) + 6\mathbf{Mod}(i, N_{CBPS})\right\} \tag{2.4}
$$

$$
T(i) = S\left\{\mathbf{Floor}\left(\frac{i}{N_{Tint}}\right) + 10\mathbf{Mod}(i, N_{Tint})\right\} \tag{2.5}
$$

where $U(i)$ is the input of the symbol interleaver, $S(i)$ is the output of the symbol interleaver and hence the input of the tone interleaver, $T(i)$ is the output of the tone interleaver, the index $i = 0, ..., 6N_{CBPS} - 1$, $\mathbf{Floor(.)}$ and $\mathbf{Mod(.)}$ denotes the floor and modulo functions, respectively, N_{CBPS}, the number of bit per OFDM symbol, follows Table 2.1, and $N_{Tint} = N_{CBPS}/10$.
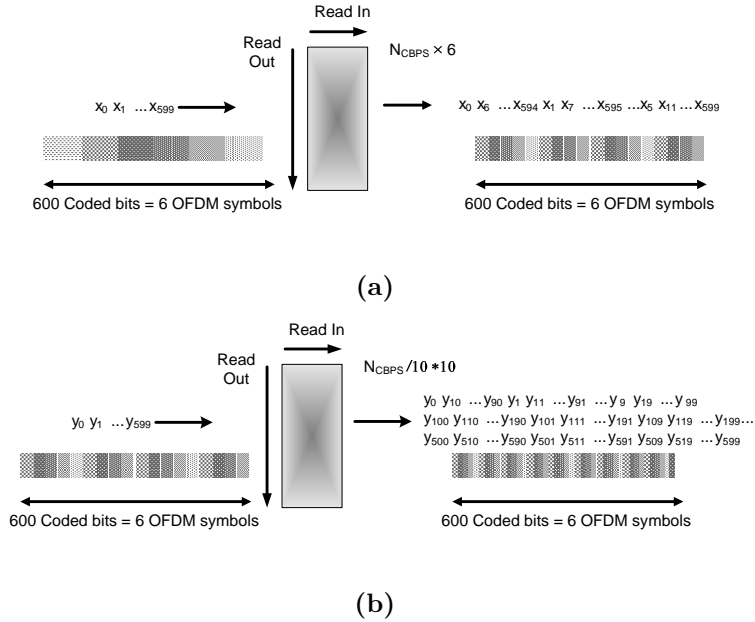
Figure 2.7: **(a) Symbol interleaver; (b) Tone Interleaver.**

Figure 2.7 illustrates the bit interleaving operation. Six hundred bits $x_0, x_1, ..., x_{599}$,

16

equivalently to six OFDM symbols, are input to the symbol interleaver that produces the output in the pattern $x_0, x_6, ...x_{594}, x_1, x_7, ..., x_{595}, ..., x_5, x_{11}, ..., x_{599}$. These output bits, now denoted as $y_0, y_1, ..., y_{599}$, are input to the tone interleaver that produces the output in the pattern $y_0, y_{10}, ...y_{90}, y_1, y_{11}, ..., y_{91}, ..., y_{509}, y_{519}, ..., y_{599}$.

2.5 Constellation Mapper

The fourth block in the baseband of the UWB transmitter is the constellation mapper, in which OFDM subcarriers are modulated using QPSK modulation. An input binary sequence is now converted into a complex-valued sequence according to Gray-coded constellation mapping as shown in Figure 2.8. Based on a pair of
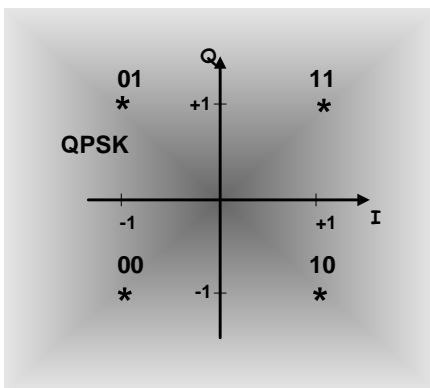
Figure 2.8: **QPSK constellation bit encoding.**

input bits, we determine the in-phase and quadrature values denoted as I and Q, respectively. Their relation follows Table 2.3. From these I and Q values, complex-valued sequence d are obtained as

$$d = (I + jQ)K_{MOD} \tag{2.6}$$

where $j = \sqrt{-1}$ is an imagine number and $K_{MOD} = \frac{1}{\sqrt{2}}$ normalizes d to unit energy.

Input bits (b_1, b_0)	I_{out}	Q_{out}
0,0	-1	-1
0,1	-1	1
1,0	1	-1
1,1	1	1

Table 2.3: **QPSK encoding.**

2.6 OFDM Modulation

The complex-valued sequence generated from the constellation mapper is ready for the OFDM modulation. The sequence in series is now converted to parallel, and the pilots, guards, and nulls are also inserted to the OFDM symbols before IFFT is taken. Each OFDM symbol contains 128 subcarriers. The duration for the OFDM symbol is $T_S = 242.42$ nsec. After that, the cyclic prefix used to eliminate the ISI is pre-appended to the OFDM symbol and the guard interval used to ensure a smooth transition between two adjacent OFDM symbols is appended. The cyclic prefix and the guard interval are filled with zeros (such a cyclic prefix is called zero-trailing). The duration of the cyclic prefix is $T_C = 60.61$ nsec, equivalently to 32 subcarriers. The duration of the guard interval is $T_G = 9.47$ nsec, equivalently to 5 subcarriers.

Among the 128 subcarriers of the OFDM symbol, one hundred data tones are used to transmit information. Twelve pilot tones are used to ensure the coherent detection robust against frequency offset and phase noise. Ten guard tones are used for a number of purposes, including relaxing the specifications on transmit and

receive filters. There are also six null tones. The positions of these tones are shown in Figure 2.9.
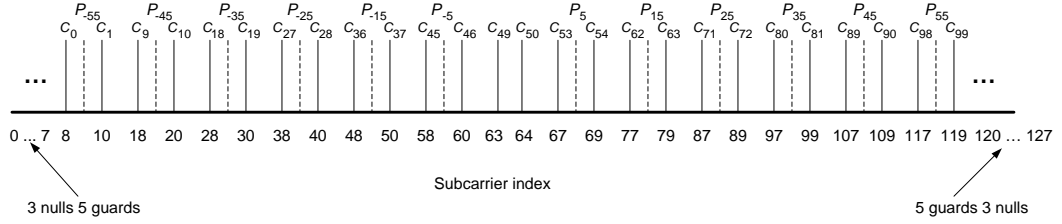
Figure 2.9: **Subcarrier frequency allocation.**

For modes with data rates 80 Mbps or lower, the complex-valued sequence is divided into groups of 50 complex numbers. The data tones c_n in Figure 2.9 for the kth OFDM symbol relate to the complex-valued sequence d as

$$c_{n,k} = d_{n+50k}$$

$$c_{(n+50),k} = d^*_{(49-n)+50k} \qquad (2.7)$$

where $n = 0, 1, ..., 49$, and $k = 0, 1, ..., N_{SYM} - 1$ with N_{SYM} denoting the number of OFDM symbols. Since the same information is transmitted twice using two subcarriers, we obtain the frequency diversity with a spreading gain factor of two for these modes.

For modes with data rates larger than 80 Mbps, the complex-valued sequence is divided into groups of 100 complex numbers. The data tones c_n in Figure 2.9 for the kth OFDM symbol relate to the complex-valued sequence d as

$$c_{n,k} = d_{n+100k} \qquad (2.8)$$

where $n = 0, 1, ..., 99$ and also $k = 0, 1, ..., N_{SYM} - 1$. In these modes, we have no frequency diversity gain since each subcarrier conveys different information.

Figure 2.9 also shows the positions for the pilots, denoted as P_n where

$$P_n = \begin{cases} \frac{1+j}{\sqrt{2}} & n = 15, 45 \\ \frac{-1-j}{\sqrt{2}} & n = 5, 25, 35, 55 \\ 0 & \text{o.w.} \end{cases} \qquad (2.9)$$

For modes with data rates less than 106.67 Mbps, $P_{n,k} = P^*_{-n,k}$ and for modes with data rates 106.67 Mbps or higher, $P_{n,k} = P_{-n,k}$ where $n = $ -5, -15, -25, -35, -45, -55. The P_n is further BPSK modulated by a pseudo-random binary sequence p_l to prevent the generation of spectral lines, where $p_{0...127} = \{$ 1, 1, 1, 1, -1, -1, -1, 1, -1, -1, -1, -1, 1, 1, -1, 1, -1, -1, 1, 1, -1, 1, 1, -1, 1, 1, 1, 1, 1, 1, -1, 1, 1, 1, -1, 1, 1, -1, -1, 1, 1, 1, 1, -1, 1, -1, -1, -1, 1, -1, 1, -1, -1, 1, 1, 1, 1, 1, -1, -1, 1, 1, -1, -1, 1, -1, 1, -1, 1, 1, -1, -1, -1, -1, 1, -1, -1, 1, -1, 1, 1, 1, 1, -1, 1, -1, 1, -1, 1, -1, -1, -1, -1, -1, 1, -1, 1, 1, -1, 1, -1, 1, 1, 1, -1, -1, 1, -1, -1, -1, 1, 1, 1, -1, -1, -1, -1, -1, -1, -1 $\}$.

The ten guards in the kth OFDM symbol take values of

$$P_{n,k} = p_{mod(k+l,127)} \frac{1+j}{\sqrt{2}} \text{ for } l = 0, 1, 2, 3, 4 \text{ and } n = 57 + l \qquad (2.10)$$

where p_l is the pseudo-random binary sequence above. For modes with data rates less than 106.67 Mbps, $P_{n,k} = P^*_{-n,k}$ and for modes with data rates 106.67 Mbps or higher, $P_{n,k} = P_{-n,k}$ where $n = $ -57, ..., -61.

2.7 Frequency and Temporal Diversity

In Section 2.6, we have seen that frequency diversity gain is obtained for modes with data rates 80 Mbps or lower by using two subcarriers to transmit the same

information. These subcarriers are in symmetric conjugate positions (see Eq. (2.7)), which make these subcarriers as less correlated as possible (we will demonstrate this in Chapter 3). To obtain temporal diversity with a gain factor of two, the same OFDM symbol is transmitted twice using different subbands. Figure 2.10 illustrates

(a)   (b)

(c)
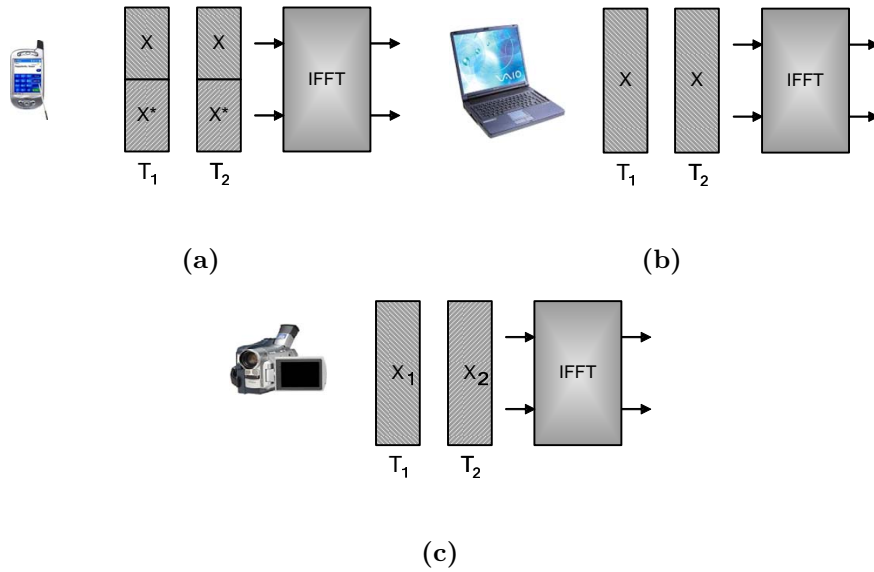
Figure 2.10: **(a) High-rate modes; (b) Middle-rate modes; (c) Low-rate modes.**

how we can obtain different overall spreading gain for different data-rate modes. For modes with data rates from 53.3 to 80 Mbps, denoted as low-rate modes, we have both time and frequency spreading, i.e., that the same information is transmitted four times, and thus we obtain a gain factor of 4. For modes with data rates from 106.7 to 200 Mbps, denoted as middle-rate modes, we have only time spreading. All of the subcarriers are used to transmit different information. The information is transmitted twice in the time domain, thus we obtain a gain factor of 2. Finally, for modes with data rates 320 Mbps or higher, denoted as high-rate modes, we have no spreading gain, i.e., that the subcarriers and time slots are used to transmit different

21

information.

Chapter 3

Performance Analysis of the MB-OFDM UWB System

3.1 Introduction

In this chapter, we present the performance analysis of the MB-OFDM UWB system. Because OFDM transmission technique is sensitive to frequency and timing synchronization, we would like to learn the system performance in different synchronization conditions. Particularly, we consider the following four synchronization scenarios:

1. Perfect frequency and timing synchronization,

2. Imperfect timing synchronization,

3. Imperfect frequency synchronization, and

4. Imperfect frequency and timing synchronization.

As we have seen in Chapter 2, the baseband of the MB-OFDM UWB system contains two main blocks: a channel coding (including the bit-interleaver) and an OFDM modulation. As illustrated in Figure 3.1, a transmitted binary sequence is input into the channel encoder. Redundancy is added to the sequence to improve the SNR for a better detection at the receiver. For our MB-OFDM UWB system, this process is done through the convolutional coding and puncturing. The bit-interleaver
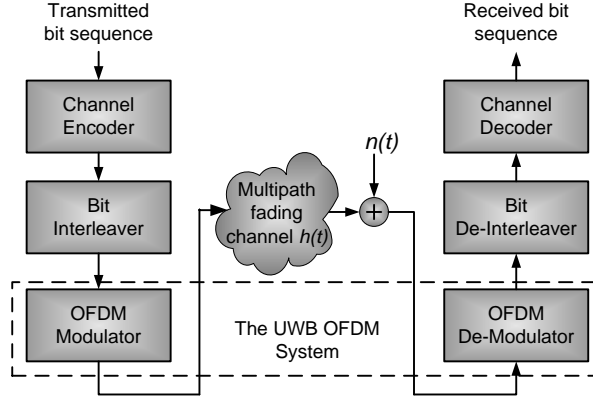
Figure 3.1: **The MB-OFDM UWB system model.**

is used to prevent burst errors. After that, the binary sequence is modulated in the OFDM modulation and transmitted through the multipath fading channel with AWGN. At the receiver, after the OFDM demodulation, we obtain a binary sequence with a certain bit error probability. The average bit error probability is determined as in previous section. This binary sequence is input into the bit-deinterleaver to obtain an output sequence, which is then filled with dummy "zero" metrics in the de-puncturing process. After that, hard-decision Viterbi decoding is applied to obtain the received binary sequence.

As a result, the system performance can be analyzed in two stages. In the first stage, we only consider the performance of the OFDM modulation block, and we will denote this block as the OFDM system in this analysis. Two metrics used to measure the performance are the degradation ratio and the average bit error probability. The first metric measures the relative performance, i.e., the performance in the imperfect synchronization to the performance in the perfect one. The second metric measures the absolute performance, i.e., the fraction of transmission bits wrong at

the receiver. Based on the average bit error probability obtained from analyzing the OFDM system, we can determine the performance bound of the entire MB-OFDM UWB system. The performance bound requires the knowledge about the channel codes such as the free distance and the weight spectrum. Unfortunately, we do not have the information. However, we will show how to obtain the performance bound when the information is available.

The content of this chapter is as follows. After this introduction section, we will introduce the IEEE 802.15.3a channel standard in Section 3.2. The standard specifies the channel conditions the UWB system works with. The performance analysis of the OFDM system will be presented in Section 3.3. In this section, we will first introduce the system model and the assumptions employed in the analysis. The introduction is presented in Subsection 3.3.1. Since the system is working in the multipath delay channel, the fading and interferences arise. Therefore, we will next derive the expressions for the fading term, the intercarrier interference (ICI) and the intersymbol interference (ISI) in Subsection 3.3.2. These expressions help us to obtain the variances of the fading term and the interferences. The derivation of the variances is presented in Subsection 3.3.3. In Subsection 3.3.4, we will define the average SNR and the performance degradation ratio of the system. The average bit error probability of the OFDM system will be presented next in Subsection 3.3.5. Since the MB-OFDM UWB system inherits three data-rate modes corresponding to different spreading gain factors, as we have seen in Chapter 2, we will derive the expressions of the average bit error probability in different data-rate modes. Based on the average bit error probability, we will show how to obtain the performance

bound of the entire MB-OFDM UWB system in Section 3.4. In the last section, Section 3.5, we will present the numerical and simulated results.

3.2 IEEE 802.15.3a Channel Standard

The UWB standard channel models specified in the IEEE 802.15.3a [10] are derived from the Saleh-Valenzuela (SV) model with some minor modifications due to clustering phenomenon. There are four different UWB standard channel models, denoted as CM1, CM2, CM3, and CM4, which are based on the line-of-sight (LOS) multipath channel condition and the distance between the transmitter and the receiver. CM1 corresponds to the LOS condition with distance of 0 to 4 meters while CM2, CM3, and CM4 are based on the non-LOS (NLOS) condition. The transmission distances in CM2 and CM3 are from 0 to 4 meters and from 4 to 10 meters, respectively. The transmission distance in CM4 is also from 4 to 10 meters but with an extreme NLOS condition.

In general, the channel impulse response can be expressed as [10]

$$h(t) = \chi \sum_{l=0}^{L} \sum_{k=0}^{K} \alpha_{k,l} \delta(t - T_l - \tau_{k,l}) \tag{3.1}$$

where $\alpha_{k,l}$ are the multipath gain coefficients, T_l is the delay of the lth cluster, $\tau_{k,l}$ is the delay of the kth ray in the lth cluster, $\delta(.)$ is the Dirac's delta function, and χ represents the log-normal shadowing. For the simplicity of the analysis, we will not consider χ in the expression of $h(t)$. In Eq. (3.1), the cluster arrival times T_l's and the ray arrival times $\tau_{k,l}$'s within each cluster are modelled as time of arrivals in Poisson processes with rate Λ and λ (where $\lambda > \Lambda$) [10], respectively. Thus they are

the l- and k-Erlang random variables with parameters Λ and λ, respectively. Notice that, for a p-Erlang random variable X with a parameter λ_X, [18]

$$f_X(x) = \frac{\lambda_X e^{-\lambda_X x}(\lambda_X x)^{p-1}}{(p-1)!} \text{ for } x > 0 \text{ and } p \geq 1 \qquad (3.2)$$

is the probabilistic density function (PDF), and

$$M_X(s) = E\left\{e^{sX}\right\} = \frac{\lambda_X^p}{(\lambda_X - s)^p} \text{ for } p \geq 1 \qquad (3.3)$$

is the moment generating function (MGF). The amplitude of the multipath gain coefficient can follow the log-normal distribution, the Nakagami distribution, or the Rayleigh distribution while the phase is uniformly distributed over $[0, 2\pi)$ [19]. In this thesis, we follow [19] to use Rayleigh distribution for the amplitude of the channel coefficient since it provides the insight of the performance of the UWB system. As a result, the multipath gain coefficients $\alpha_{k,l}$'s are modelled as statistically independent, zero-mean, complex Gaussian random variables whose variance is [10]

$$\Omega_{k,l} = E\left\{|\alpha_{k,l}|^2 \mid T_l, \tau_{k,l}\right\} = \Omega_{0,0} e^{-\frac{T_l}{\Gamma} - \frac{\tau_{k,l}}{\gamma}}. \qquad (3.4)$$

where Γ and γ are the decay factors of the cluster and ray, respectively. Table 3.1 presents the model parameters Λ, λ, Γ, and γ.

Observations: The expression for the channel impulse response in Eq. (3.1) is very general. It does not reflect the insight of the channel models. To be more precise, we realize that in all channel models, $\tau_{0,l} = 0$ for all l, i.e., that the first ray in the lth cluster arrives when the lth cluster arrives. In CM1, where the LOS condition is applied, $T_0 = 0$, i.e, that the 0th cluster always arrives at time 0 and hence the

	CM1	CM2	CM3	CM4
Λ (1/nsec)	0.0233	0.4	0.0667	0.0667
λ (1/nsec)	2.5	0.5	2.1	2.1
Γ	7.1	5.5	14.000	24.000
γ	4.3	6.7	7.9	12

Table 3.1: **Model parameters.**

arrival time of the 0th cluster is deterministic. In other channel models, i.e., CM2, CM3, and CM4 where the NLOS condition is applied, T_0 does not exist since all arrival times T_l's are random. As a result, we offer to rewrite the expression for the channel impulse response for CM1 as

$$
h(t) = \alpha_{0,0}\delta(t) + \sum_{k=1}^{K}\alpha_{k,0}\delta(t - \tau_{k,0})
$$
$$
+ \sum_{l=1}^{L}\alpha_{0,l}\delta(t - T_l) + \sum_{l=1}^{L}\sum_{k=1}^{K}\alpha_{k,l}\delta(t - T_l - \tau_{k,l}). \tag{3.5}
$$

The channel impulse response for CM2, CM3, and CM4 takes the form of Eq. (3.5) without the first two terms because these channel models do not inherit the LOS condition.

The above observation is important for the performance analysis of the UWB system. As we have seen in Eqs. (3.2) and (3.3), the index for the p-Erlang random variable starts from $p = 1$, not from 0 as shown in Eq. (3.1). In addition, the expression of the channel in Eq. (3.5) provides the insight of the channel models, i.e., LOS vs. Non-LOS condition. Therefore, by ignoring the above observation, the performance analysis of the UWB system would possess errors. In Section 3.3,

we will perform the analysis based on the channel model CM1. Expressions of quantities of interest for channel models CM2, CM3, and CM4 can be obtained from those in CM1 by ignoring the terms corresponding to the first two terms in Eq. (3.5). For simplicity, we will employ both expressions for the channel models in our performance analysis. Particularly, we will use the expression in Eq. (3.1) when deriving the expressions of the fading term, the ICI, and the ISI and use the expression in Eq. (3.5) when deriving the expressions for their variances. In the next section, the performance analysis of the OFDM system will be presented.

3.3 Performance Analysis of the OFDM System

3.3.1 System Model and Assumptions

We will consider the performance analysis of the OFDM system in the baseband continuous-time. Figure 3.2 shows the baseband model of the OFDM system. We consider an input data sequence $\{c_{0,i}, c_{1,i}, ..., c_{n,i}, ..., c_{N-1,i}\}$ with the OFDM
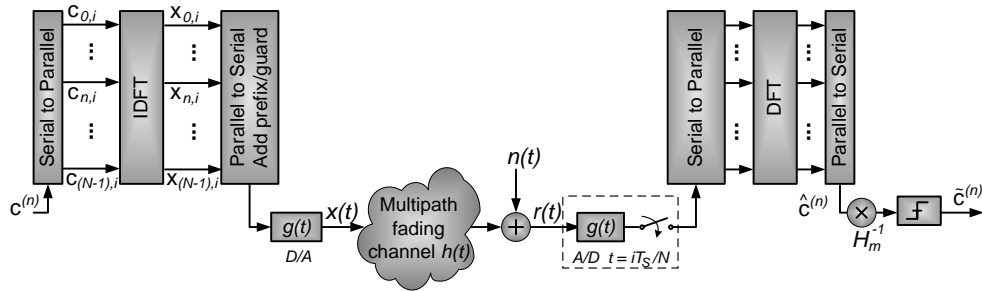
Figure 3.2: **OFDM system model.**

symbol index i and the subcarrier index n. N is the number of subcarriers. The transmitted OFDM symbol can be generated by using an N-point IFFT. Before

being transmitted, the useful OFDM symbols with a duration T_S are pre-appended by a cyclic prefix (actually zero-trailing, i.e., that the prefix is filled with zeros) with a duration T_C to eliminate the intersymbol interference (ISI) and appended by a guard interval with a duration T_G to ensure the transfer between two consecutive OFDM symbols [8]. The output of the IFFT is

$$x_i(t) = \frac{1}{T_S} \sum_{n=0}^{N-1} c_{n,i} g(t - iT_S') e^{\frac{j2\pi n(t-iT_S')}{T_S}} \quad \text{for} -\infty \leq i \leq \infty \tag{3.6}$$

where $T_S' = T_C + T_S + T_G$ is the duration of the transmitted OFDM symbol, and

$$g(t) = \begin{cases} 1 & T_C \leq t \leq T_C + T_S \\ 0 & \text{o.w} \end{cases} \tag{3.7}$$

is the rectangular pulse.

The transmitted signal $x(t) = \sum_{i=-\infty}^{i=\infty} x_i(t)$ travels through the UWB channel whose the continuous-time impulse response is

$$h(t) = \sum_{l=0}^{L} \sum_{k=0}^{K} \alpha_{k,l} \delta(t - T_l - \tau_{k,l})$$

as described in Eq. (3.1) of Section 3.2. The received signal $r(t)$ is the sum of the output $y(t)$ of the channel and the additive white Gaussian noise (AWGN) $n(t)$, i.e,

$$r(t) = y(t) + n(t) = \sum_{i=-\infty}^{i=\infty} y_i(t) + n(t) \tag{3.8}$$

where

$$\begin{aligned} y_i(t) &= x_i(t) \star h(t) \\ &= \frac{1}{T_S} \sum_{n=0}^{N-1} c_{n,i} \sum_{l=0}^{L} \sum_{k=0}^{K} \alpha_{k,l}\, g(t - iT_S' - T_l - \tau_{k,l}) e^{\frac{j2\pi n(t-iT_S'-T_l-\tau_{k,l})}{T_S}} \end{aligned} \tag{3.9}$$

30

is the output of the channel corresponding to the OFDM symbol $x_i(t)$. Notice that in Eq. (3.9), $(\star)$ denotes the convolution.

At the receiver, the frequency and timing synchronization may not be perfect. The imperfection of frequency synchronization results in a carrier-frequency offset $\Delta f = f_r - f_t$ due to the mismatch between the oscillators of the transmitter and the receiver. Likewise, the error in timing synchronization causes the timing offset τ due to the misplacement of the FFT window. Figure 3.3 illustrates the imperfection of frequency and timing synchronization. In this analysis, we will consider a number of

(a)   (b)
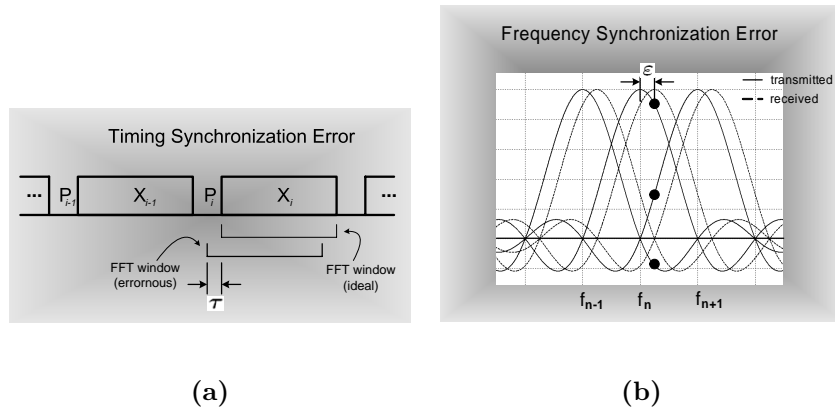
Figure 3.3: **(a) Timing synchronization error; (b) Frequency synchronization error.**

cases relating to frequency and timing synchronization. Particularly, we will study the performance of the system for the following four cases:

1. Perfect frequency and timing synchronization,

2. Imperfect timing synchronization,

3. Imperfect frequency synchronization, and

4. Imperfect frequency and timing synchronization.

The demodulated signal $\hat{c}_{m,i}$ can be obtained by integrating the received signal corresponding to the subcarrier m in the interval $t \in [iT'_S+T_C+\tau,\ iT'_S+T_C+T_S+\tau]$ as follows

$$\hat{c}_{m,i} = \int_{iT'_S+T_C-\tau}^{iT'_S+T_C+T_S-\tau} r(t)e^{-j2\pi(f_{t,m}+\Delta f)(t-iT'_S)}dt \qquad (3.10)$$

where $f_{t,m}$ is the transmitter carrier frequency corresponding to the subcarrier m. Let ε be the relative carrier-frequency offset. Then

$$\varepsilon = \frac{\Delta f}{1/T_S} = \Delta f T_S. \qquad (3.11)$$

Applying the change of variable $t' = t + \tau$ in Eq. (3.10) and using Eq. (3.11) yield

$$\begin{aligned}
\hat{c}_{m,i} &= \int_{iT'_S+T_C}^{iT'_S+T_C+T_S} r(t-\tau)e^{\frac{-j2\pi(m+\varepsilon)(t-iT'_S-\tau)}{T_S}}dt \\
&= \int_{iT'_S+T_C}^{iT'_S+T_C+T_S} y_i(t-\tau)e^{\frac{-j2\pi(m+\varepsilon)(t-iT'_S-\tau)}{T_S}}dt \\
&\quad + \sum_{i'\neq i}\int_{iT'_S+T_C}^{iT'_S+T_C+T_S} y_{i'}(t-\tau)e^{\frac{-j2\pi(m+\varepsilon)(t-iT'_S-\tau)}{T_S}}dt \\
&\quad + \int_{iT'_S+T_C}^{iT'_S+T_C+T_S} n(t)e^{\frac{-j2\pi(m+\varepsilon)(t-iT'_S-\tau)}{T_S}}dt \\
&= A_{m,i} + \hat{c}_{m,i}^{ISI} + n_{m,i} \qquad (3.12)
\end{aligned}$$

where we have defined $A_{m,i}$, $\hat{c}_{m,i}^{ISI}$, and $n_{m,i}$ as the first, second, and third term in Eq. (3.12). $A_{m,i}$ contains the information about the ith OFDM symbols, and hence contains the desired symbol $c_{m,i}$ with its fading term H_m and the interference $\hat{c}_{m,i}^{ICI}$ from other subcarriers in the same OFDM symbol, thus called the ICI. In other words,

$$A_{m,i} = c_{m,i}H_m + \hat{c}_{m,i}^{ICI}. \qquad (3.13)$$

Also in Eq. (3.12), $\hat{c}_{m,i}^{ISI}$ is the interference from adjacent OFDM symbols, thus called the ISI and $n_{m,i} \sim CN(0, N_0)$ is the AWGN. Consequently, we can rewrite

the demodulated signal as

$$\hat{c}_{m,i} = c_{m,i}H_m + \hat{c}_{m,i}^{ICI} + \hat{c}_{m,i}^{ISI} + n_{m,i}. \tag{3.14}$$

Depending on different conditions of frequency and timing synchronization, the fading term, the ICI, and the ISI are different. The derivations of the expressions for these terms and their variances employ the following assumptions.

- **Assumption 1:** $\tau \in (-T_C, \ T_C)$. This assumption is reasonable since the timing error usually takes place around zeros. For large timing errors τ, the performance possesses very high probability of error and hence needs not to be considered.

- **Assumption 2:** $T_l + \tau_{k,l} \leq T_S$ for all k, l. This assumption is valid because through the generation of the channel models, we observe that no delay is larger than the symbol duration T_S.

- **Assumption 3:** Let $X = T_l + \tau_{k,l} - T$ and $l_0 = \lfloor \Lambda T \rfloor$ where T representing time is deterministic and $\lfloor . \rfloor$ represents the floor function. T_l and $\tau_{k,l}$ are random variables, so is X. l_0 represents the average number of cluster arrivals at time T since Λ is the cluster arrival rate. Then $X > 0 \Leftrightarrow l \geq l_0 + 1$. This assumption means that if the time of arrival of the lth cluster $T_l < T$, then all rays in that cluster arrive assumedly at a time less than T; in other words, $T_l + \tau_{k,l} < T$. This assumption helps to simplify the derivations of the quantities of interest but still maintains the nature of the problem.

- **Assumption 4:** All the transmitted symbols $c_{n,i}$ are independent and iden-

33

tically distributed (i.i.d) with the symbol energy E_s. Since two bits form a QPSK symbol in our system, $E_s = 2E_b$ where E_b is the bit energy.

- **Assumption 5:** The channel, the transmitted symbols, and the AWGN are mutually independent. This assumption helps to simplify the derivation of the performance of the system.

- **Assumption 6:** The number of arrival clusters and rays is infinite. This assumption is valid since the tail in exponential decay does not contribute much to the total sum. This assumption helps to simplify the expressions for the variances of the quantities of interest.

Using the above assumptions, in the next section, we will derive the expression for the fading term, the ICI, and the ISI of the OFDM system.

3.3.2 Expressions for the Fading Term, the ICI, and the ISI

We will derive the expressions for the fading term, the ICI and the ISI based on the demodulated signal $\hat{c}_{m,i}$ in Eq. (3.12). First, the expressions for the fading term and the ICI will be obtained through the evaluation of the quantity $A_{m,i}$ in Eq. (3.12). The evaluation will be presented in **A**. After that, the expression of the ISI will be derived by itself. The derivation will be presented in **B**. For simplicity, we will use the expression for the channel impulse response in Eq. (3.1) for the derivation.

A. Derivations of H_m and $\hat{c}_{m,i}^{ICI}$

From Eq. (3.12),

$$A_{m,i} = \int_{iT_S'+T_C}^{iT_S'+T_C+T_S} y_i(t-\tau)e^{\frac{-j2\pi(m+\varepsilon)(t-iT_S'-\tau)}{T_S}}\, dt \tag{3.15}$$

Substituting $y_i(t)$ from Eq. (3.9) into Eq. (3.15) and applying the change of variable

in t, we have

$$A_{m,i} = \frac{1}{T_S}\sum_{n=0}^{N-1} c_{n,i}\sum_{l=0}^{L}\sum_{k=0}^{K}\alpha_{k,l}\int_{T_C}^{T_C+T_S} g(t-T_l-\tau_{k,l}-\tau)$$
$$\times e^{\frac{j2\pi n(t-T_l-\tau_{k,l}-\tau)}{T_S}}\, e^{\frac{-j2\pi(m+\varepsilon)(t-\tau)}{T_S}}\, dt \tag{3.16}$$

where the rectangular pulse

$$g(t-T_l-\tau_{k,l}-\tau) = \begin{cases} 1 & T_C+T_l+\tau_{k,l}+\tau \le t \le T_C+T_S+T_l+\tau_{k,l}+\tau \\ \\ 0 & \text{o.w} \end{cases} \tag{3.17}$$

Let us define

$$I_{k,l}^c \triangleq \int_{T_C}^{T_C+T_S} g(t-T_l-\tau_{k,l}-\tau)e^{\frac{j2\pi n(t-T_l-\tau_{k,l}-\tau)}{T_S}}\, e^{\frac{-j2\pi(m+\varepsilon)(t-\tau)}{T_S}}\, dt \tag{3.18}$$

in Eq. (3.16). When the timing error is negative, i.e., $\tau < 0$, the quantity X,

defined as $X = T_l + \tau_{k,l} + \tau$, is negative for some l, k and positive otherwise. By

using Assumption 3, the integral $I_{k,l}^c$ can be expressed as

$$I_{k,l}^c = \begin{cases} I_{k,l}^1 & \text{for } l > l_0 \\ \\ I_{k,l}^2 & \text{for } l \le l_0 \end{cases} \tag{3.19}$$

where $l_o = \lfloor -\Lambda\tau \rfloor$. For the first case, when $l > l_0$

$$\begin{aligned} I_{k,l}^1 &= \int_{T_C+T_l+\tau_{k,l}+\tau}^{T_C+T_S} e^{\frac{j2\pi n(t-T_l-\tau_{k,l}-\tau)}{T_S}}\, e^{\frac{-j2\pi(m+\varepsilon)(t-\tau)}{T_S}}\, dt \\ &= T_S\, e^{\frac{j2\pi(n-m-\varepsilon)T_C}{T_S}}\, e^{\frac{j2\pi(m+\varepsilon)\tau}{T_S}}\left(\frac{e^{-j2\pi\varepsilon}e^{\frac{-j2\pi n(T_l+\tau_{k,l}+\tau)}{T_S}} - e^{\frac{-j2\pi(m+\varepsilon)(T_l+\tau_{k,l}+\tau)}{T_S}}}{j2\pi(n-m-\varepsilon)}\right). \end{aligned}$$
$$\tag{3.20}$$

For the second case, when $l \leq l_0$

$$
\begin{aligned}
I_{k,l}^2 &= \int_{T_C}^{T_C+T_S+T_l+\tau_{k,l}+\tau} e^{\frac{j2\pi n(t-T_l-\tau_{k,l}-\tau)}{T_S}} e^{\frac{-j2\pi(m+\varepsilon)(t-\tau)}{T_S}} \, dt \\
&= T_S \, e^{\frac{j2\pi(n-m-\varepsilon)T_C}{T_S}} e^{\frac{j2\pi(m+\varepsilon)\tau}{T_S}} \left(\frac{e^{-j2\pi\varepsilon} e^{\frac{-j2\pi(m+\varepsilon)(T_l+\tau_{k,l}+\tau)}{T_S}} - e^{\frac{-j2\pi n(T_l+\tau_{k,l}+\tau)}{T_S}}}{j2\pi(n-m-\varepsilon)} \right).
\end{aligned}
$$

(3.21)

Using Eqs. (3.20) and (3.21) in Eq. (3.16) and separating the terms corresponding to the transmission symbol $c_{m,i}$ from others yield

$$
\begin{aligned}
H_m &= e^{\frac{-j2\pi\varepsilon T_C}{T_S}} e^{\frac{j2\pi(m+\varepsilon)\tau}{T_S}} \\
&\times \left[\sum_{l=0}^{l_0} \sum_{k=0}^{K} \alpha_{k,l} e^{\frac{-j2\pi m(T_l+\tau_{k,l}+\tau)}{T_S}} \left(\frac{e^{-j2\pi\varepsilon} e^{\frac{-j2\pi\varepsilon(T_l+\tau_{k,l}+\tau)}{T_S}} - 1}{-j2\pi\varepsilon} \right) \right. \\
&\left. + \sum_{l=l_0+1}^{L} \sum_{k=0}^{K} \alpha_{k,l} e^{\frac{-j2\pi m(T_l+\tau_{k,l}+\tau)}{T_S}} \left(\frac{e^{-j2\pi\varepsilon} - e^{\frac{-j2\pi\varepsilon(T_l+\tau_{k,l}+\tau)}{T_S}}}{-j2\pi\varepsilon} \right) \right]
\end{aligned}
$$

(3.22)

and

$$
\begin{aligned}
\hat{c}_{m,i}^{ICI} &= \sum_{n\neq m} c_{n,i} e^{\frac{j2\pi(n-m-\varepsilon)T_C}{T_S}} e^{\frac{j2\pi(m+\varepsilon)\tau}{T_S}} \\
&\times \left[\sum_{l=0}^{l_0} \sum_{k=0}^{K} \alpha_{k,l} \left(\frac{e^{-j2\pi\varepsilon} e^{\frac{-j2\pi(m+\varepsilon)(T_l+\tau_{k,l}+\tau)}{T_S}} - e^{\frac{-j2\pi n(T_l+\tau_{k,l}+\tau)}{T_S}}}{j2\pi(n-m-\varepsilon)} \right) \right. \\
&\left. + \sum_{l=l_0+1}^{L} \sum_{k=0}^{K} \alpha_{k,l} \left(\frac{e^{-j2\pi\varepsilon} e^{\frac{-j2\pi n(T_l+\tau_{k,l}+\tau)}{T_S}} - e^{\frac{-j2\pi(m+\varepsilon)(T_l+\tau_{k,l}+\tau)}{T_S}}}{j2\pi(n-m-\varepsilon)} \right) \right]
\end{aligned}
$$

(3.23)

where again $l_0 = \lfloor -\Lambda\tau \rfloor$.

The expressions for the fading term and the ICI in Eqs. (3.22) and (3.23) are generic. For a particular synchronization condition, the application of the expres-

sions needs the following remarks.

Remark 1: When $\tau \geq 0$ ($l_0 < 0$), the $\sum_{l=0}^{l_0}$ is invalid, and the $\sum_{l=l_0+1}^{L}$ starts with $l = 0$.

Remark 2: When $\varepsilon = 0$, i.e., the case of perfect frequency synchronization,

$$\frac{e^{-j2\pi\varepsilon}e^{\frac{-j2\pi\varepsilon(T_l+\tau_{k,l}+\tau)}{T_S}} - 1}{-j2\pi\varepsilon}$$

and

$$\frac{e^{-j2\pi\varepsilon} - e^{\frac{-j2\pi\varepsilon(T_l+\tau_{k,l}+\tau)}{T_S}}}{-j2\pi\varepsilon}$$

are undefined (we have $\frac{0}{0}$). However,

$$\lim_{\varepsilon\to 0}\frac{e^{-j2\pi\varepsilon}e^{\frac{-j2\pi\varepsilon(T_l+\tau_{k,l}+\tau)}{T_S}} - 1}{-j2\pi\varepsilon} = T_S + T_l + \tau_{k,l} + \tau$$

$$\lim_{\varepsilon\to 0}\frac{e^{-j2\pi\varepsilon} - e^{\frac{-j2\pi\varepsilon(T_l+\tau_{k,l}+\tau)}{T_S}}}{-j2\pi\varepsilon} = T_S - T_l - \tau_{k,l} - \tau$$

and they will be used in Eq. (3.22) instead.

Remark 3: When $n = m + \varepsilon$, i.e., the case of imperfect frequency synchronization with a multiple-subcarrier offset (ε is an integer),

$$\frac{e^{-j2\pi\varepsilon}e^{\frac{-j2\pi(m+\varepsilon)(T_l+\tau_{k,l}+\tau)}{T_S}} - e^{\frac{-j2\pi n(T_l+\tau_{k,l}+\tau)}{T_S}}}{j2\pi(n - m - \varepsilon)}$$

and

$$\frac{e^{-j2\pi\varepsilon}e^{\frac{-j2\pi n(T_l+\tau_{k,l}+\tau)}{T_S}} - e^{\frac{-j2\pi(m+\varepsilon)(T_l+\tau_{k,l}+\tau)}{T_S}}}{j2\pi(n - m - \varepsilon)}$$

are undefined (we have $\frac{0}{0}$). However,

$$\lim_{n\to(m+\varepsilon)} \frac{e^{-j2\pi\varepsilon}e^{\frac{-j2\pi(m+\varepsilon)(T_l+\tau_{k,l}+\tau)}{T_S}} - e^{\frac{-j2\pi n(T_l+\tau_{k,l}+\tau)}{T_S}}}{j2\pi(n-m-\varepsilon)} =$$

$$\frac{1}{T_S}e^{\frac{-j2\pi(m+\varepsilon)(T_l+\tau_{k,l}+\tau)}{T_S}}(T_S+T_l+\tau_{k,l}+\tau)$$

$$\lim_{n\to(m+\varepsilon)} \frac{e^{-j2\pi\varepsilon}e^{\frac{-j2\pi n(T_l+\tau_{k,l}+\tau)}{T_S}} - e^{\frac{-j2\pi(m+\varepsilon)(T_l+\tau_{k,l}+\tau)}{T_S}}}{j2\pi(n-m-\varepsilon)} =$$

$$\frac{1}{T_S}e^{\frac{-j2\pi(m+\varepsilon)(T_l+\tau_{k,l}+\tau)}{T_S}}(T_S-T_l-\tau_{k,l}-\tau)$$

and they will be used in Eq. (3.23) instead.

B. Derivations of $\hat{c}_{m,i}^{ISI}$

From Eq. (3.12),

$$\hat{c}_{m,i}^{ISI} = \sum_{i'\neq i} \int_{iT_S'+T_C}^{iT_S'+T_C+T_S} y_{i'}(t-\tau)e^{\frac{-j2\pi(m+\varepsilon)(t-iT_S'-\tau)}{T_S}}\,\mathrm{dt} \qquad (3.24)$$

is the inter-symbol interference. Based on Assumption 1 where $-T_C < \tau$, future OFDM symbols do not interfere with the current i^{th} symbol. Moreover, the combination of Assumptions 1 and 2 where $\max(T_l+\tau_{k,l})+\tau < T_S'$ with $T_S' = T_C+T_S+T_G$ suggests that the ith OFDM symbol receives the ISI only from the $(i-1)^{\text{th}}$ OFDM symbol. Therefore, we rewrite the ISI as

$$\hat{c}_{m,i}^{ISI} = \int_{iT_S'+T_C}^{iT_S'+T_C+T_S} y_{i-1}(t-\tau)e^{\frac{-j2\pi(m+\varepsilon)(t-iT_S'-\tau)}{T_S}}\,\mathrm{dt} \qquad (3.25)$$

Substituting $y_{i-1}(t)$ from Eq. (3.9) into Eq. (3.25) and applying the change of variable in t yield

$$\hat{c}_{m,i}^{ISI} = \frac{1}{T_S}\sum_{n=0}^{N-1}c_{n,i-1}\sum_{l=1}^{L}\sum_{k=1}^{K}\alpha_{k,l}\int_{T_C}^{T_C+T_S} g(t-T_l-\tau_{k,l}-\tau+T_S')$$

$$\times e^{\frac{j2\pi n(t-T_l-\tau_{k,l}-\tau+T_C+T_G)}{T_S}}e^{\frac{-j2\pi(m+\varepsilon)(t-\tau)}{T_S}}\,\mathrm{dt} \qquad (3.26)$$

where the rectangular pulse

$$g(t - T_l - \tau_{k,l} - \tau + T'_S) = \begin{cases} 1 & T_l + \tau_{k,l} + \tau - T_S - T_G \leq t \leq T_l + \tau_{k,l} + \tau - T_G \\ 0 & \text{o.w} \end{cases} .$$

(3.27)

Let us define

$$I^s_{k,l} \triangleq \int_{T_C}^{T_C+T_S} g(t - T_l - \tau_{k,l} - \tau + T'_S) e^{\frac{j2\pi n(t - T_l - \tau_{k,l} - \tau + T_C + T_G)}{T_S}} e^{\frac{-j2\pi(m+\varepsilon)(t-\tau)}{T_S}} \, dt$$

(3.28)

in Eq. (3.26). Based on Assumptions 1 and 2, $T_l + \tau_{k,l} + \tau < T'_S \ \forall \ k, l$. Thus

$T_l + \tau_{k,l} + \tau - T_G < T_S + T_C$ and $T_l + \tau_{k,l} + \tau - T_S - T_G < T_C \ \forall \ k, l$. However,

$T_l + \tau_{k,l} + \tau - T_G \geq T_C$ for only some k, l. Hence

$$\begin{aligned} I^s_{k,l} &= \int_{T_C}^{T_l+\tau_{k,l}+\tau-T_G} e^{\frac{j2\pi n(t - T_l - \tau_{k,l} - \tau + T_C + T_G)}{T_S}} e^{\frac{-j2\pi(m+\varepsilon)(t-\tau)}{T_S}} \, dt \\ &= T_S \, e^{\frac{j2\pi(n-m-\varepsilon)T_C}{T_S}} e^{\frac{j2\pi(m+\varepsilon)\tau}{T_S}} \left(\frac{e^{\frac{-j2\pi(m+\varepsilon)(T_l+\tau_{k,l}+\tau-T_C-T_G)}{T_S}} - e^{\frac{-j2\pi n(T_l+\tau_{k,l}+\tau-T_C-T_G)}{T_S}}}{j2\pi(n-m-\varepsilon)} \right) . \end{aligned}$$

(3.29)

for $l > l_0$ where $l_0 = \lfloor \Lambda(T_G + T_C - \tau) \rfloor$ by using Assumption 3. Using Eq. (3.29) in

Eq. (3.26) yields

$$\begin{aligned} \hat{c}^{ISI}_{m,i} &= \sum_{n=0}^{N-1} c_{n,i-1} e^{\frac{j2\pi(n-m-\varepsilon)T_C}{T_S}} e^{\frac{j2\pi(m+\varepsilon)\tau}{T_S}} \\ &\quad \times \sum_{l=l_0+1}^{L} \sum_{k=0}^{K} \alpha_{k,l} \left(\frac{e^{\frac{-j2\pi(m+\varepsilon)(T_l+\tau_{k,l}+\tau-T_C-T_G)}{T_S}} - e^{\frac{-j2\pi n(T_l+\tau_{k,l}+\tau-T_C-T_G)}{T_S}}}{j2\pi(n-m-\varepsilon)} \right) . \end{aligned}$$

(3.30)

Remark 4: Since $l_0 = \lfloor \Lambda(T_G + T_C - \tau) \rfloor$, l_0 for positive τ is smaller than that for

negative τ. Clearly, the positive τ causes more ISI to the current i^{th} symbol.

39

The expression for the ISI in Eq. (3.30) is generic. For a particular synchronization condition, the application of the expression needs the following remark.

Remark 5: When $n = m + \varepsilon$, i.e., the case of imperfect frequency synchronization with a multiple-subcarrier offset (ε is an integer),

$$\frac{e^{\frac{-j2\pi(m+\varepsilon)(T_l+\tau_{k,l}+\tau-T_C-T_G)}{T_S}} - e^{\frac{-j2\pi n(T_l+\tau_{k,l}+\tau-T_C-T_G)}{T_S}}}{j2\pi(n-m-\varepsilon)}$$

is undefined (we have $\frac{0}{0}$). However,

$$\lim_{n\to(m+\varepsilon)} \frac{e^{\frac{-j2\pi(m+\varepsilon)(T_l+\tau_{k,l}+\tau-T_C-T_G)}{T_S}} - e^{\frac{-j2\pi n(T_l+\tau_{k,l}+\tau-T_C-T_G)}{T_S}}}{j2\pi(n-m-\varepsilon)} =$$
$$e^{\frac{-j2\pi(m+\varepsilon)(T_l+\tau_{k,l}+\tau-T_C-T_G)}{T_S}}(T_l + \tau_{k,l} + \tau - T_C - T_G)$$

and it will be used in Eq. (3.23) instead.

In the next subsection, we will present the derivation of the variances of the fading term, the ICI, and the ISI.

3.3.3   Variances of the Fading Term, the ICI, and the ISI

We are now ready to derive the variances of the fading term, the ICI, and the ISI based on their expressions in Subsection 3.3.2. Let us denote the variances of the fading term, the ICI, and the ISI as σ_H^2, σ_C^2, and σ_S^2, respectively. Because the transmitted symbols $c_{n,i}$'s and the multipath gain coefficients $\alpha_{k,l}$'s are zero-mean, the fading terms H_m, the ICI $\hat{c}_{m,i}^{ICI}$, and the ISI $\hat{c}_{m,i}^{ISI}$ are also zero-mean. Thus the variances of these terms are equal to their second moment, i.e., that $\sigma_H^2 = E\{|H_m|^2\}$, $\sigma_C^2 = E\{|\hat{c}_{m,i}^{ICI}|^2\}$, and $\sigma_H^2 = E\{|\hat{c}_{m,i}^{ISI}|^2\}$. Using Assumptions

4 and 5 and noting that the multipath gain coefficients $\alpha_{k,l}$'s are zero-mean and statistically independent, we can show that

$$
\begin{aligned}
\sigma_H^2 &= \frac{1}{4\pi^2\varepsilon^2}\sum_{l=0}^{l_0}\sum_{k=0}^{K}E\left\{|\alpha_{k,l}|^2\right.\\
&\quad\times\left[2-\left(e^{-j2\pi\varepsilon}e^{\frac{-j2\pi\varepsilon(T_l+\tau_{k,l}+\tau)}{T_S}}+e^{j2\pi\varepsilon}e^{\frac{j2\pi\varepsilon(T_l+\tau_{k,l}+\tau)}{T_S}}\right)\right]\right\}\\
&\quad+\frac{1}{4\pi^2\varepsilon^2}\sum_{l=l_0+1}^{L}\sum_{k=0}^{K}E\left\{|\alpha_{k,l}|^2\right.\\
&\quad\times\left.\left[2-\left(e^{-j2\pi\varepsilon}e^{\frac{j2\pi\varepsilon(T_l+\tau_{k,l}+\tau)}{T_S}}+e^{j2\pi\varepsilon}e^{\frac{-j2\pi\varepsilon(T_l+\tau_{k,l}+\tau)}{T_S}}\right)\right]\right\},
\end{aligned}
$$

$$
\begin{aligned}
\sigma_C^2 &= E_s\sum_{n\neq m}\frac{1}{4\pi^2(n-m-\varepsilon)^2}\sum_{l=0}^{l_0}\sum_{k=0}^{K}E\left\{|\alpha_{k,l}|^2\right.\\
&\quad\times\left[2-\left(e^{-j2\pi\varepsilon}e^{\frac{j2\pi(n-m-\varepsilon)(T_l+\tau_{k,l}+\tau)}{T_S}}+e^{j2\pi\varepsilon}e^{\frac{-j2\pi(n-m-\varepsilon)(T_l+\tau_{k,l}+\tau)}{T_S}}\right)\right]\right\}\\
&\quad+E_s\sum_{n\neq m}\frac{1}{4\pi^2(n-m-\varepsilon)^2}\sum_{l=l_0+1}^{L}\sum_{k=0}^{K}E\left\{|\alpha_{k,l}|^2\right.\\
&\quad\times\left.\left[2-\left(e^{-j2\pi\varepsilon}e^{\frac{-j2\pi(n-m-\varepsilon)(T_l+\tau_{k,l}+\tau)}{T_S}}+e^{j2\pi\varepsilon}e^{\frac{j2\pi(n-m-\varepsilon)(T_l+\tau_{k,l}+\tau)}{T_S}}\right)\right]\right\},
\end{aligned}
$$

and

$$
\begin{aligned}
\sigma_S^2 &= E_s\sum_{n=0}^{N-1}\frac{1}{4\pi^2(n-m-\varepsilon)^2}\times\sum_{l=l_0+1}^{L}\sum_{k=0}^{K}E\left\{|\alpha_{k,l}|^2\right.\\
&\quad\times\left.\left[2-\left(e^{\frac{-j2\pi(n-m-\varepsilon)(T_l+\tau_{k,l}+\tau-T_C-T_G)}{T_S}}+e^{\frac{j2\pi(n-m-\varepsilon)(T_l+\tau_{k,l}+\tau-T_C-T_G)}{T_S}}\right)\right]\right\}.
\end{aligned}
$$

By conditioning on T_l and $\tau_{k,l}$ and using Eq. (3.4), we finally obtain

$$
\begin{aligned}
\sigma_H^2 &= \frac{1}{4\pi^2\varepsilon^2}\sum_{l=0}^{l_0}\sum_{k=0}^{K}E\left\{\Omega_{0,0}e^{-\frac{T_l}{\Gamma}-\frac{\tau_{k,l}}{\gamma}}\right.\\
&\quad\times\left[2-\left(e^{-j2\pi\varepsilon}e^{\frac{-j2\pi\varepsilon(T_l+\tau_{k,l}+\tau)}{T_S}}+e^{j2\pi\varepsilon}e^{\frac{j2\pi\varepsilon(T_l+\tau_{k,l}+\tau)}{T_S}}\right)\right]\right\}\\
&\quad+\frac{1}{4\pi^2\varepsilon^2}\sum_{l=l_0+1}^{L}\sum_{k=0}^{K}E\left\{\Omega_{0,0}e^{-\frac{T_l}{\Gamma}-\frac{\tau_{k,l}}{\gamma}}\right.
\end{aligned}
$$

$$\times \left[2 - \left(e^{-j2\pi\varepsilon} e^{\frac{j2\pi\varepsilon(T_l + \tau_{k,l} + \tau)}{T_S}} + e^{j2\pi\varepsilon} e^{\frac{-j2\pi\varepsilon(T_l + \tau_{k,l} + \tau)}{T_S}} \right) \right] \right\},$$

$$(3.31)$$

$$\begin{aligned}
\sigma_C^2 &= E_s \sum_{n \neq m} \frac{1}{4\pi^2 (n - m - \varepsilon)^2} \sum_{l=0}^{l_0} \sum_{k=0}^{K} E \left\{ \Omega_{0,0} e^{-\frac{T_l}{\Gamma} - \frac{\tau_{k,l}}{\gamma}} \right. \\
&\quad \times \left[2 - \left(e^{-j2\pi\varepsilon} e^{\frac{j2\pi(n-m-\varepsilon)(T_l + \tau_{k,l} + \tau)}{T_S}} + e^{j2\pi\varepsilon} e^{\frac{-j2\pi(n-m-\varepsilon)(T_l + \tau_{k,l} + \tau)}{T_S}} \right) \right] \right\} \\
&\quad + E_s \sum_{n \neq m} \frac{1}{4\pi^2 (n - m - \varepsilon)^2} \sum_{l=l_0+1}^{L} \sum_{k=0}^{K} E \left\{ \Omega_{0,0} e^{-\frac{T_l}{\Gamma} - \frac{\tau_{k,l}}{\gamma}} \right. \\
&\quad \times \left[2 - \left(e^{-j2\pi\varepsilon} e^{\frac{-j2\pi(n-m-\varepsilon)(T_l + \tau_{k,l} + \tau)}{T_S}} + e^{j2\pi\varepsilon} e^{\frac{j2\pi(n-m-\varepsilon)(T_l + \tau_{k,l} + \tau)}{T_S}} \right) \right] \right\},
\end{aligned}$$

$$(3.32)$$

and

$$\begin{aligned}
\sigma_S^2 &= E_s \sum_{n=0}^{N-1} \frac{1}{4\pi^2 (n - m - \varepsilon)^2} \times \sum_{l=l_0+1}^{L} \sum_{k=0}^{K} E \left\{ \Omega_{0,0} e^{-\frac{T_l}{\Gamma} - \frac{\tau_{k,l}}{\gamma}} \right. \\
&\quad \times \left[2 - \left(e^{\frac{-j2\pi(n-m-\varepsilon)(T_l + \tau_{k,l} + \tau - T_C - T_G)}{T_S}} + e^{\frac{j2\pi(n-m-\varepsilon)(T_l + \tau_{k,l} + \tau - T_C - T_G)}{T_S}} \right) \right] \right\}.
\end{aligned}$$

$$(3.33)$$

The remaining task is to evaluate the expressions of the variances of the fading term, the ICI, and the ISI in Eqs. (3.31), (3.32), and (3.33). For the derivation, we need to take in account the observation about the channel impulse response in Section 3.2. Particularly, we will use the expression of the channel impulse response in Eq. (3.5). Furthermore, the derivation will employ the remarks, Remarks 1-3 and 5, in Subsection 3.3.2 and Assumption 6 in Subsection 3.3.1.

Let us define the following four quantities.

$$A_1(T, l_0, \Lambda, \Gamma, \lambda, \gamma) \triangleq \sum_{l=l_0+1}^{\infty} \sum_{k=1}^{\infty} E \left\{ \Omega_{0,0} e^{-\frac{T_l}{\Gamma} - \frac{\tau_{k,l}}{\gamma}} (T_l + \tau_{k,l} - T)^2 \right\} \qquad (3.34)$$

$$A_2(T, p_0, \lambda_X, \gamma_X) \triangleq \sum_{p=p_0+1}^{\infty} E\left\{\Omega_{0,0} e^{-\frac{X}{\gamma_X}} (X - T)^2\right\} \tag{3.35}$$

$$B_1(T, n, m, \varepsilon, \varepsilon', l_0, \Lambda, \Gamma, \lambda, \gamma) \triangleq \sum_{l=l_0+1}^{\infty} \sum_{k=1}^{\infty} E\left\{\Omega_{0,0} e^{-\frac{T_l}{\Gamma} - \frac{\tau_{k,l}}{\gamma}} \right.$$
$$\times \left[2 - \left(e^{-j2\pi\varepsilon'} e^{\frac{-j2\pi(n-m-\varepsilon)(T_l+\tau_{k,l}-T)}{T_S}}\right.\right.$$
$$\left.\left.\left. + e^{j2\pi\varepsilon'} e^{\frac{j2\pi(n-m-\varepsilon)(T_l+\tau_{k,l}-T)}{T_S}}\right)\right]\right\} \tag{3.36}$$

and

$$B_2(T, n, m, \varepsilon, \varepsilon', p_0, \lambda_X, \gamma_X) \triangleq \sum_{p=p_0+1}^{\infty} E\left\{\Omega_{0,0} e^{-\frac{X}{\gamma_X}} \right.$$
$$\times \left[2 - \left(e^{-j2\pi\varepsilon'} e^{\frac{-j2\pi(n-m-\varepsilon)(X-T)}{T_S}}\right.\right.$$
$$\left.\left.\left. + e^{j2\pi\varepsilon'} e^{\frac{j2\pi(n-m-\varepsilon)(X-T)}{T_S}}\right)\right]\right\} \tag{3.37}$$

where $E\{.\}$ denotes the expectation. In the above equations, T_l, $\tau_{k,l}$, and X are the times of arrivals in Poisson processes whose rates are Λ, λ, and λ_X and decay factors are Γ, γ, and γ_X, respectively. The PDF and the MGF of these random variables follow Eqs. (3.2) and (3.3).

Clearly, $B_1(.)$ relates directly to the expressions in Eqs. (3.31), (3.32), and (3.33). The introduction of $A_1(.)$ and $A_2(.)$ is due to Remarks 2, 3, and 4 in Subsection 3.3.2 while the introduction of $A_2(.)$ and $B_2(.)$ is due to the observation about the channel in Section 3.2. The variances of interest will be separated in term of $A_1(.)$, $A_2(.)$, $B_1(.)$, and $B_2(.)$ with different values of T, n, m, ε, ε'. Thus the evaluation of the four quantities should be the next task. In **A**, we will present the derivation of the $A_1(.)$ and $A_2(.)$. After that the expressions for $B_1(.)$ and $B_2(.)$ will be evaluated in **B**. In **C**, we will provide the expressions for the variances of interest

43

in term of $A_1(.)$, $A_2(.)$, $B_1(.)$, and $B_2(.)$. In these derivations, we will employ the fact that for a p-Erlang random variable

$$E\left\{X^n e^{sX}\right\} = \frac{d^{(n)} G_X(s)}{ds} = \frac{(p+n-1)!}{(p-1)!} \frac{\lambda_X^p}{(\lambda_X - s)^{p+n}}.$$

Thus

$$E\left\{X e^{sX}\right\} = \frac{p\lambda_X^p}{(\lambda_X - s)^{p+1}} \tag{3.38}$$

and

$$E\left\{X^2 e^{sX}\right\} = \frac{p(p+1)\lambda_X^p}{(\lambda_X - s)^{p+2}}. \tag{3.39}$$

A. Derivations of $A_1(.)$ and $A_2(.)$

Since T_l and $\tau_{k,l}$ are statistically independent,

$$
\begin{aligned}
A_1(T, l_0, \Lambda, \Gamma, \lambda, \gamma) &= \Omega_{0,0} \sum_{l=l_0+1}^{\infty} \sum_{k=1}^{\infty} \left[E\left\{T_l^2 e^{-\frac{T_l}{\Gamma}}\right\} E\left\{e^{-\frac{\tau_{k,l}}{\gamma}}\right\} \right. \\
&\quad + E\left\{e^{-\frac{T_l}{\Gamma}}\right\} E\left\{\tau_{k,l}^2 e^{-\frac{\tau_{k,l}}{\gamma}}\right\} + T^2 E\left\{e^{-\frac{T_l}{\Gamma}}\right\} E\left\{e^{-\frac{\tau_{k,l}}{\gamma}}\right\} \\
&\quad + E\left\{T_l e^{-\frac{T_l}{\Gamma}}\right\} E\left\{\tau_{k,l} e^{-\frac{\tau_{k,l}}{\gamma}}\right\} - 2TE\left\{T_l e^{-\frac{T_l}{\Gamma}}\right\} E\left\{e^{-\frac{\tau_{k,l}}{\gamma}}\right\} \\
&\quad \left. - 2TE\left\{e^{-\frac{T_l}{\Gamma}}\right\} E\left\{\tau_{k,l} e^{-\frac{\tau_{k,l}}{\gamma}}\right\} \right].
\end{aligned}
$$

Using Eqs. (3.3), (3.38), and (3.39) for the expectations yields

$$
\begin{aligned}
A_1(T, l_0, \Lambda, \Gamma, \lambda, \gamma) &= \Omega_{0,0} \left[\sum_{l=l_0+1}^{\infty} \frac{l(l+1)\Lambda^l}{(\Lambda + \frac{1}{\Gamma})^{l+2}} \sum_{k=1}^{\infty} \frac{\lambda^k}{(\lambda + \frac{1}{\gamma})^k} \right. \\
&\quad + \sum_{l=l_0+1}^{\infty} \frac{\Lambda^l}{(\Lambda + \frac{1}{\Gamma})^l} \sum_{k=1}^{\infty} \frac{k(k+1)\lambda^k}{(\lambda + \frac{1}{\gamma})^{k+2}} \\
&\quad + T_S^2 \sum_{l=l_0+1}^{\infty} \frac{\Lambda^l}{(\Lambda + \frac{1}{\Gamma})^l} \sum_{k=1}^{\infty} \frac{\lambda^k}{(\lambda + \frac{1}{\gamma})^k} \\
&\quad + 2 \sum_{l=l_0+1}^{\infty} \frac{l\Lambda^l}{(\Lambda + \frac{1}{\Gamma})^{l+1}} \sum_{k=1}^{\infty} \frac{k\lambda^k}{(\lambda + \frac{1}{\gamma})^{k+1}}
\end{aligned}
$$

44

$$-2T \sum_{l=l_0+1}^{\infty} \frac{l\Lambda^l}{(\Lambda + \frac{1}{\Gamma})^{l+1}} \sum_{k=1}^{K} \frac{\lambda^k}{(\lambda + \frac{1}{\gamma})^k}$$

$$-2T \sum_{l=l_0+1}^{\infty} \frac{\Lambda^l}{(\Lambda + \frac{1}{\Gamma})^l} \sum_{k=1}^{\infty} \frac{k\lambda^k}{(\lambda + \frac{1}{\gamma})^{k+1}} \Bigg].$$

To obtain the expression for $A_1(.)$, we will employ the following remark about geometric series.

Remark: For $\beta = \frac{\lambda_X \gamma_X}{\lambda_X \gamma_X + 1}$ $(|\beta| < 1)$,

$$\sum_{p=0}^{\infty} \beta^p = \frac{1}{1-\beta} = (\lambda_X \gamma_X + 1)$$

$$\sum_{p=0}^{\infty} p\beta^p = \frac{\beta}{(1-\beta)^2} = \lambda_X \gamma_X (\lambda_X \gamma_X + 1)$$

$$\sum_{p=0}^{\infty} p(p+1)\beta^n = \frac{2\beta}{(1-\beta)^3} = 2\lambda_X \gamma_X (\lambda_X \gamma_X + 1)^2.$$

Hence

$$\sum_{p=p_0+1}^{\infty} \beta^n = \beta^{p_0+1} \sum_{p=0}^{\infty} \beta^p = f_1(p_0, \lambda_X, \gamma_X) \tag{3.40}$$

$$\sum_{p=p_0+1}^{\infty} p\beta^p = \beta^{p_0+1} \left[\sum_{p=0}^{\infty} p\beta^p + (p_0+1) \sum_{p=0}^{\infty} \beta^p \right]$$

$$= (\lambda_X \gamma_X + 1) f_2(p_0, \lambda_X, \gamma_X) \tag{3.41}$$

$$\sum_{p=p_0+1}^{\infty} p(p+1)\beta^p = \beta^{p_0+1} \left[\sum_{p=0}^{\infty} p(p+1)\beta^p + 2(p_0+1) \sum_{p=0}^{\infty} p\beta^p \right.$$

$$\left. + (p_0+1)(p_0+2) \sum_{p=0}^{\infty} \beta^p \right]$$

$$= (\lambda_X \gamma_X + 1)^2 f_3(p_0, \lambda_X, \gamma_X) \tag{3.42}$$

where we have defined

$$f_1(p_0, \lambda_X, \gamma_X) \triangleq \frac{(\lambda_X \gamma_X)^{p_0+1}}{(\lambda_X \gamma_X + 1)^{p_0+1}} (\lambda_X \gamma_X + 1) \tag{3.43}$$

$$f_2(p_0, \lambda_X, \gamma_X) \triangleq \frac{(\lambda_X \gamma_X)^{p_0+1}}{(\lambda_X \gamma_X + 1)^{p_0+1}} (\lambda_X \gamma_X + p_0 + 1) \tag{3.44}$$

$$f_3(p_0, \lambda_X, \gamma_X) \triangleq \frac{(\lambda_X \gamma_X)^{p_0+1}}{(\lambda_X \gamma_X + 1)^{p_0+2}} \left[2\lambda_X \gamma_X (\lambda_X \gamma_X + 1) \right.$$

$$\left. + 2(p_0 + 1)\lambda_X \gamma_X + (p_0 + 1)(p_0 + 2) \right]. \tag{3.45}$$

Using Eqs. (3.40), (3.41), and (3.42) and applying simplifications yield

$$A_1(T, l_0, \Lambda, \Gamma, \lambda, \gamma) = \Omega_{0,0} \left[\Gamma^2 f_3(l_0, \Lambda, \Gamma) f_1(0, \lambda, \gamma) + \gamma^2 f_1(l_0, \Lambda, \Gamma) f_3(0, \lambda, \gamma) \right.$$

$$+ T^2 f_1(l_0, \Lambda, \Gamma) f_1(0, \lambda, \gamma) + 2\Gamma \gamma f_2(l_0, \Lambda, \Gamma) f_2(0, \lambda, \gamma)$$

$$\left. - 2T\Gamma f_2(l_0, \Lambda, \Gamma) f_1(0, \lambda, \gamma) - 2T\gamma f_1(l_0, \Lambda, \Gamma) f_2(0, \lambda, \gamma) \right].$$

$$\tag{3.46}$$

Similarly, by using Eqs. (3.3), (3.38), and (3.39) and applying simplifications we can show that

$$A_2(T, p_0, \lambda_X, \gamma_X) = \Omega_{0,0} \left[\gamma_X^2 f_3(p_0, \lambda_X, \gamma_X) + T^2 f_1(p_0, \lambda_X, \gamma_X) \right.$$

$$\left. - 2T\gamma_X f_2(p_0, \lambda_X, \gamma_X) \right]. \tag{3.47}$$

B. Derivations of $B_1(.)$ and $B_2(.)$

In the same manner of the derivation of the $A_1(.)$ and $A_2(.)$, since T_l and $\tau_{k,l}$ are statistically independent,

$$B_1(T, n, m, \varepsilon, \varepsilon', l_0, \Lambda, \Gamma, \lambda, \gamma) = \Omega_{0,0} \left[2 \sum_{l=l_0+1}^{\infty} E\left\{ e^{-\frac{T_l}{\Gamma}} \right\} \sum_{k=1}^{\infty} E\left\{ e^{-\frac{\tau_{k,l}}{\gamma}} \right\} \right.$$

$$- e^{-j2\pi\varepsilon'} e^{\frac{j2\pi(n-m-\varepsilon)T}{T_S}} \sum_{l=l_0+1}^{\infty} E\left\{ e^{\left(-\frac{1}{\Gamma} - \frac{j2\pi(n-m-\varepsilon)}{T_S}\right)T_l} \right\}$$

$$\left. \times \sum_{k=1}^{\infty} E\left\{ e^{\left(-\frac{1}{\gamma} - \frac{j2\pi(n-m-\varepsilon)}{T_S}\right)\tau_{k,l}} \right\} \right.$$

$$- e^{-j2\pi\varepsilon'} e^{\frac{j2\pi(n-m-\varepsilon)T}{T_S}} \sum_{l=l_0+1}^{\infty} E\left\{ e^{\left(-\frac{1}{\Gamma} + \frac{j2\pi(n-m-\varepsilon)}{T_S}\right)T_l} \right\}$$

$$\times \sum_{k=1}^{\infty} E\left\{ e^{\left(-\frac{1}{\gamma} + \frac{j2\pi(n-m-\varepsilon)}{T_S}\right)\tau_{k,l}} \right\} \Bigg].$$

If X is a p-Erlang random varilable, then from Eq. (3.3),

$$E\left\{ e^{\left(-\frac{1}{\gamma_X} \pm \frac{j2\pi(n-m-\varepsilon)}{T_S}\right)X} \right\} = \frac{\lambda_X^p}{\left(\lambda_X + \frac{1}{\gamma_X} \mp \frac{j2\pi(n-m-\varepsilon)}{T_S}\right)^p}$$

$$= \left(\beta_X e^{\pm j\theta_X}\right)^p$$

where we have defined

$$\beta_X \triangleq \frac{\lambda_X}{\sqrt{\left(\lambda_X + \frac{1}{\gamma_X}\right)^2 + \frac{4\pi^2(n-m-\varepsilon)^2}{T_S^2}}} \tag{3.48}$$

and

$$\theta_X \triangleq \arctan\left(\frac{2\pi(n-m-\varepsilon)}{T_S} \frac{\gamma_X}{\lambda_X\gamma_X + 1}\right). \tag{3.49}$$

In addition, for $\beta = \beta_X e^{\pm j\theta_X}$ where $|\beta_X| < 1$, we can show that

$$\sum_{p=0}^{\infty} \left(\beta_X e^{\pm j\theta_X}\right)^p = \frac{1 - \beta_X e^{\mp j\theta_X}}{1 + \beta_X^2 - 2\beta_X \cos\theta_X}.$$

Hence

$$\sum_{p=p_0+1}^{\infty} E\left\{ e^{\left(-\frac{1}{\gamma_X} \pm \frac{j2\pi(n-m-\varepsilon)}{T_S}\right)X} \right\} = \beta_X^{p_0+1} e^{\pm j(p_0+1)\theta_X} \frac{1 - \beta_X e^{\mp j\theta_X}}{1 + \beta_X^2 - 2\beta_X \cos\theta_X} \tag{3.50}$$

by Eq. (3.40).

Using Eqs. (3.3) and (3.50) yields

$$B_1(T, n, m, \varepsilon, \varepsilon', l_0, \Lambda, \Gamma, \lambda, \gamma) = 2\Omega_{0,0} f_1(l_0, \Lambda, \Gamma) f_1(0, \lambda, \lambda) - \Omega_{0,0}\beta_T^{l_0+1}\beta_\tau$$

$$\times \Bigg[\frac{e^{-j2\pi\varepsilon'} e^{\frac{j2\pi(n-m-\varepsilon)T}{T_S}} e^{-j(l_0+1)\theta_T} e^{-j\theta_\tau} \left(1 - \beta_T e^{j\theta_T}\right)\left(1 - \beta_\tau e^{j\theta_\tau}\right)}{(1 + \beta_T^2 - 2\beta_T \cos\theta_T)(1 + \beta_\tau^2 - 2\beta_\tau \cos\theta_\tau)}$$

$$+ \frac{e^{j2\pi\varepsilon'} e^{\frac{-j2\pi(n-m-\varepsilon)T}{T_S}} e^{j(l_0+1)\theta_T} e^{j\theta_\tau} \left(1 - \beta_T e^{-j\theta_T}\right)\left(1 - \beta_\tau e^{-j\theta_\tau}\right)}{(1 + \beta_T^2 - 2\beta_T \cos\theta_T)(1 + \beta_\tau^2 - 2\beta_\tau \cos\theta_\tau)} \Bigg].$$

where $f_1(.)$ has been defined in Eq. (3.43). After the simplification, we eventually obtain

$$
\begin{aligned}
B_1(T, n, m, \varepsilon, \varepsilon', l_0, \Lambda, \Gamma, \lambda, \gamma) &= 2\Omega_{0,0}f_1(l_0, \Lambda, \Gamma)f_1(0, \lambda, \lambda) - 2\Omega_{0,0}\beta_T^{l_0+1}\beta_\tau \\
&\times \left[\frac{\cos\left((l_0+1)\theta_T + \theta_\tau - \frac{2\pi(n-m-\varepsilon)T}{T_S} + 2\pi\varepsilon'\right)}{(1+\beta_T^2 - 2\beta_T\cos\theta_T)(1+\beta_\tau^2 - 2\beta_\tau\cos\theta_\tau)} \right. \\
&- \frac{\beta_\tau\cos\left((l_0+1)\theta_T - \frac{2\pi(n-m-\varepsilon)T}{T_S} + 2\pi\varepsilon'\right)}{(1+\beta_T^2 - 2\beta_T\cos\theta_T)(1+\beta_\tau^2 - 2\beta_\tau\cos\theta_\tau)} \\
&- \frac{\beta_T\cos\left(l_0\theta_T + \theta_\tau - \frac{2\pi(n-m-\varepsilon)T}{T_S} + 2\pi\varepsilon'\right)}{(1+\beta_T^2 - 2\beta_T\cos\theta_T)(1+\beta_\tau^2 - 2\beta_\tau\cos\theta_\tau)} \\
&+ \left. \frac{\beta_T\beta_\tau\cos\left(l_0\theta_T - \frac{2\pi(n-m-\varepsilon)T}{T_S} + 2\pi\varepsilon'\right)}{(1+\beta_T^2 - 2\beta_T\cos\theta_T)(1+\beta_\tau^2 - 2\beta_\tau\cos\theta_\tau)} \right].
\end{aligned}
$$

(3.51)

In the same manner, using Eqs. (3.4) and (3.50), we can show that

$$
\begin{aligned}
B_2(T, n, m, \varepsilon, \varepsilon', p_0, \lambda_X, \gamma_X) &= 2\Omega_{0,0}f_1(p_0, \lambda_X, \gamma_X) - 2\Omega_{0,0}\beta_X^{p_0+1} \\
&\times \left[\frac{\cos\left((p_0+1)\theta_X - \frac{2\pi(n-m-\varepsilon)T}{T_S} + 2\pi\varepsilon'\right)}{1+\beta_X^2 - 2\beta_X\cos\theta_X} \right. \\
&- \left. \beta_X\frac{\cos\left(p_0\theta_X - \frac{2\pi(n-m-\varepsilon)T}{T_S} + 2\pi\varepsilon'\right)}{1+\beta_X^2 - 2\beta_X\cos\theta_X} \right]
\end{aligned}
$$

(3.52)

where $f_1(.)$, β_X and θ_X have been defined in Eq. (3.43), Eqs. (3.48) and (3.49), respectively.

C. Expressions for the Variances of the Fading Term, the ICI, the ISI

Using the expressions for $A_1(.)$, $A_2(.)$, $B_1(.)$, and $B_2(.)$ obtained in Subsections A and B, we derive the expressions for the variances of interest in term of the four

48

quantities. In the following, we will present the final results of the derivation. The variances are listed based on the frequency and timing synchronization conditions.

1. **Perfect frequency and timing synchronization, i.e., $\varepsilon = 0$ and $\tau = 0$:**

$$
\sigma_H^2 = \Omega_{0,0} + \frac{1}{T_S^2} A_2(T_S, 0, \lambda, \gamma) + \frac{1}{T_S^2} A_2(T_S, 0, \Lambda, \Gamma) + \frac{1}{T_S^2} A_1(T_S, 0, \Lambda, \Gamma, \lambda, \gamma)
$$

$$
\sigma_C^2 = E_s \sum_{n \neq m} \frac{1}{4\pi^2(n-m)^2} [B_2(0, n, m, 0, 0, 0, \lambda, \gamma)
$$
$$
+ B_2(0, n, m, 0, 0, 0, \Lambda, \Gamma) + B_1(0, n, m, 0, 0, 0, \Lambda, \Gamma, \lambda, \gamma)]
$$

$$
\sigma_S^2 = E_s \left[\frac{1}{T_S^2} A_2(T_C + T_G, p_0, \Lambda, \Gamma) + \frac{1}{T_S^2} A_1(T_C + T_G, p_0) \right.
$$
$$
+ \sum_{n \neq m} \frac{1}{4\pi^2(n-m)^2} [B_2(T_C + T_G, n, m, 0, 0, p_0, \Lambda, \Gamma)
$$
$$
\left. + B_1(T_C + T_G, n, m, 0, 0, p_0, \Lambda, \Gamma, \lambda, \gamma)] \right]
$$

where $p_0 = \lfloor \Lambda(T_G + T_C - \tau) \rfloor$.

Remark 6: When the UWB system is working in CM2, CM3, and CM4, the non-LOS condition is applied. Thus $l = 0$, corresponding to the arrival time of the first cluster T_0, does not exist since all clusters arrive randomly (See Observation in Section 3.2). In this case, the first two terms in the σ_H^2 expression and the first term in the σ_C^2 expression do not exist.

2. **Imperfect timing synchronization, i.e., $\varepsilon = 0$ and $\tau \neq 0$:**

$$
\sigma_H^2 = \Omega_{0,0} \frac{(\tau + T_S)^2}{T_S^2} + \frac{1}{T_S^2} A_2(-T_S - \tau, 0, \lambda, \gamma)
$$
$$
+ \frac{1}{T_S^2} A_2(-T_S - \tau, 0, \Lambda, \Gamma) - \frac{1}{T_S^2} A_2(-T_S - \tau, l_0, \Lambda, \Gamma)
$$

49

$$+\frac{1}{T_S^2}A_2(T_S - \tau, l_0, \Lambda, \Gamma) + \frac{1}{T_S^2}A_1(-T_S - \tau, 0, \Lambda, \Gamma, \lambda, \gamma)$$

$$-\frac{1}{T_S^2}A_1(-T_S - \tau, l_0, \Lambda, \Gamma, \lambda, \gamma) + \frac{1}{T_S^2}A_1(T_S - \tau, l_0, \Lambda, \Gamma, \lambda, \gamma)$$

where $l_0 = \lfloor -\Lambda\tau \rfloor$.

Remark 7: In the case of positive timing error $\tau \geq 0$, Remark 1 in Subsection 3.3.2 will be used. Particularly, all terms containing $-T_S$ (the 2nd, 3rd, 4th, 6th, and 7th) are invalid and $l_0 = 0$.

$$
\begin{aligned}
\sigma_C^2 &= E_s \sum_{n \neq m} \frac{1}{4\pi^2(n-m)^2} \left[2\Omega_{0,0} \left(1 - \cos\frac{2\pi(n-m)\tau}{T_S} \right) \right. \\
&\quad + B_2(-\tau, n, m, 0, 0, 0, \lambda, \gamma) + B_2(-\tau, n, m, 0, 0, 0, \Lambda, \Gamma) \\
&\quad \left. + B_1(-\tau, n, m, 0, 0, 0, \Lambda, \Gamma, \lambda, \gamma) \right]
\end{aligned}
$$

$$
\begin{aligned}
\sigma_S^2 &= E_s \left[\frac{1}{T_S^2}A_2(T_C + T_G - \tau, p_0, \Lambda, \Gamma) + \frac{1}{T_S^2}A_1(T_C + T_G - \tau, p_0, \Lambda, \Gamma, \lambda, \gamma) \right. \\
&\quad + \sum_{n \neq m} \frac{1}{4\pi^2(n-m)^2} \left[B_2(T_C + T_G - \tau, n, m, 0, 0, p_0, \Lambda, \Gamma) \right. \\
&\quad \left. \left. + B_1(T_C + T_G - \tau, n, m, 0, 0, p_0, \Lambda, \Gamma, \lambda, \gamma) \right] \right]
\end{aligned}
$$

where $p_0 = \lfloor \Lambda(T_G + T_C - \tau) \rfloor$.

Remark 8: When the UWB system is working in CM2, CM3, and CM4, with the same reason presented in Remark 6, the first two terms in the σ_H^2 expression and in the σ_C^2 expression do not exist.

50

3. **Imperfect frequency synchronization, i.e., $\varepsilon \neq 0$ and $\tau = 0$:**

$$\sigma_H^2 = \frac{1}{4\pi^2\varepsilon^2} [2\Omega_{0,0}(1 - \cos 2\pi\varepsilon) + B_2(0,0,0,\varepsilon,\varepsilon,0,\lambda,\gamma)$$

$$+ B_2(0,0,0,\varepsilon,\varepsilon,0,\Lambda,\Gamma) + B_1(0,0,0,\varepsilon,\varepsilon,0,\Lambda,\Gamma,\lambda,\gamma)]$$

$$\sigma_C^2 = E_s \sum_{n \neq m} \frac{1}{4\pi^2(n-m-\varepsilon)^2} [2\Omega_{0,0}(1 - \cos 2\pi\varepsilon)$$

$$+ B_2(0,n,m,\varepsilon,\varepsilon,0,\lambda,\gamma) + B_2(0,n,m,\varepsilon,\varepsilon,0,\Lambda,\Gamma)$$

$$+ B_1(0,n,m,\varepsilon,\varepsilon,0,\Lambda,\Gamma,\lambda,\gamma)]$$

$$\sigma_S^2 = E_s \sum_{n=0}^{N-1} \frac{1}{4\pi^2(n-m-\varepsilon)^2} [B_2(T_C+T_G,n,m,\varepsilon,0,p_0,\Lambda,\Gamma)$$

$$+ B_1(T_C+T_G,n,m,\varepsilon,0,p_0,\Lambda,\Gamma,\lambda,\gamma)]$$

where $p_0 = \lfloor \Lambda(T_G + T_C - \tau) \rfloor$.

Remark 9: When the UWB system is working in CM2, CM3, and CM4, with the same reason presented in Remark 6, the first two terms in the σ_H^2 expression and in the σ_C^2 expression do not exist.

4. **Imperfect frequency and timing synchronization, i.e., $\varepsilon \neq 0$ and $\tau \neq 0$:**

$$\sigma_H^2 = \frac{1}{4\pi^2\varepsilon^2} \left[2\Omega_{0,0}\left(1 - \cos\left(\frac{2\pi\varepsilon\tau}{T_S} + 2\pi\varepsilon\right)\right) + B_2(-\tau,0,0,\varepsilon,-\varepsilon,0,\lambda,\gamma)\right.$$

$$+ B_2(-\tau,0,0,\varepsilon,-\varepsilon,0,\Lambda,\Gamma) - B_2(-\tau,0,0,\varepsilon,-\varepsilon,l_0,\Lambda,\Gamma)$$

$$+ B_2(-\tau,0,0,\varepsilon,\varepsilon,l_0,\Lambda,\Gamma) + B_1(-\tau,0,0,\varepsilon,-\varepsilon,0,\Lambda,\Gamma,\lambda,\gamma)$$

$$\left. - B_1(-\tau,0,0,\varepsilon,-\varepsilon,l_0,\Lambda,\Gamma,\lambda,\gamma) + B_1(-\tau,0,0,\varepsilon,\varepsilon,l_0,\Lambda,\Gamma,\lambda,\gamma)\right]$$

$$\sigma_C^2 = E_s \sum_{n \neq m} \frac{1}{4\pi^2(n-m-\varepsilon)^2} \left[2\Omega_{0,0} \left(1 - \cos\left(\frac{2\pi(n-m-\varepsilon)\tau}{T_S} - 2\pi\varepsilon \right) \right) \right.$$

$$+ B_2(-\tau, n, m, \varepsilon, -\varepsilon, 0, \lambda, \gamma) + B_2(-\tau, n, m, \varepsilon, -\varepsilon, 0, \Lambda, \Gamma)$$

$$- B_2(-\tau, n, m, \varepsilon, -\varepsilon, l_0, \Lambda, \Gamma) + B_2(-\tau, n, m, \varepsilon, \varepsilon, l_0, \Lambda, \Gamma)$$

$$+ B_1(-\tau, n, m, \varepsilon, -\varepsilon, 0, \Lambda, \Gamma, \lambda, \gamma) - B_1(-\tau, n, m, \varepsilon, -\varepsilon, l_0, \Lambda, \Gamma, \lambda, \gamma)$$

$$\left. + B_1(-\tau, n, m, \varepsilon, \varepsilon, l_0, \Lambda, \Gamma, \lambda, \gamma) \right]$$

where $l_0 = \lfloor -\Lambda\tau \rfloor$.

Remark 10: In the case of positive timing error $\tau \geq 0$, Remark 1 in Subsection 3.3.2 will be used in the above two expressions. Particularly, $l_0 = 0$ will make the 3rd and 4th terms cancel each other, likewise the 6th and 7th) terms. In addition, the $2\pi\varepsilon$ in the s^{st} term will be replaced by $-2\pi\varepsilon$, and the $-\varepsilon$ in the 2nd term will be replaced by ε.

$$\sigma_S^2 = E_s \sum_{n=0}^{N-1} \frac{1}{4\pi^2(n-m-\varepsilon)^2} \left[B_2(T_C + T_G - \tau, n, m, \varepsilon, 0, p_0, \Lambda, \Gamma) \right.$$

$$\left. + B_1(T_C + T_G - \tau, n, m, \varepsilon, 0, p_0, \Lambda, \Gamma, \lambda, \gamma) \right]$$

where $p_0 = \lfloor \Lambda(T_G + T_C - \tau) \rfloor$.

Remark 11: When the UWB sytem is working in CM2, CM3, and CM4, with the same reason presented in Remark 6, the first two terms in the σ_H^2 expression and in the σ_C^2 expression do not exist.

3.3.4 The Average Signal-to-Noise Ratio and the Performance Degradation

In previous subsection, we have derived the expressions of the variances σ_H^2, σ_C^2, and σ_S^2 of the fading term, the ICI, and the ISI, respectively. The ICI and ISI variances can be expressed as products of the symbol energy E_s and the relative variances, i.e., that $\sigma_C^2 = E_s \tilde{\sigma}_C^2$ and $\sigma_S^2 = E_s \tilde{\sigma}_S^2$. Beside the multipath effect, which causes the fading and the interferences, the received symbol is also affected by the AWGN $n_{m,i}$ whose variance is N_0. Thus the average SNR per QPSK symbol can be defined as

$$\overline{\gamma_s}(\varepsilon, \ \tau) \triangleq \frac{\sigma_H^2}{\tilde{\sigma}_C^2 + \tilde{\sigma}_S^2 + \frac{N_0}{E_s}}. \tag{3.53}$$

In addition, we also define the average SNR per bit as

$$\overline{\gamma_b}(\varepsilon, \ \tau) \triangleq \frac{\sigma_H^2}{2\tilde{\sigma}_C^2 + 2\tilde{\sigma}_S^2 + \frac{N_0}{E_b}}. \tag{3.54}$$

where $E_b = \frac{1}{2}E_s$, the energy per bit. Note that $\overline{\gamma_b}(\varepsilon, \ \tau) = \frac{1}{2}\overline{\gamma_s}(\varepsilon, \ \tau)$ We will use $\overline{\gamma_s}(\varepsilon, \ \tau)$ and $\overline{\gamma_b}(\varepsilon, \ \tau)$ to evaluate the performance of the OFDM system.

The first metric in valuating the system performance is the degradation ratio, defined as

$$D(\varepsilon, \tau) = 10 \log \frac{\overline{\gamma_s}(0, \ 0)}{\overline{\gamma_s}(\varepsilon, \ \tau)} \text{ dB}. \tag{3.55}$$

It measures the relative performance of the system, i.e., the system performance in the imperfect synchronization in comparison with the performance of the system in a perfect one. In Section 3.5, we will present and analyze the system performance degradation based on the numerical results obtained from Eq. (3.55).

The second metric in assessing the system performance is the average bit error probability, which measures the absolute performance. It is defined as a fraction of transmission bits wrong. In the next subsection, we will derive the average bit error probability corresponding different data rate modes.

3.3.5 The Average Bit Error Probability

From Eq. (3.14), the demodulated signal $\hat{c}_{m,i}$ at the subcarrier m^{th} contains the transmit symbol $c_{m,i}$ with its fading term H_m in addition to the interferences $\hat{c}_{m,i}^{ICI}$ and $\hat{c}_{m,i}^{ISI}$ and the AWGN $n_{m,i}$. Let us define

$$z_m \triangleq \hat{c}_{m,i}^{ICI} + \hat{c}_{m,i}^{ISI} + n_{m,i}. \tag{3.56}$$

as the sum of the ICI, the ISI and the AWGN. The the demodulated signal then be

$$\hat{c}_{m,i} = c_{m,i} H_m + z_m \tag{3.57}$$

where

$$
\begin{aligned}
H_m \;=\; & \frac{1}{-j2\pi\varepsilon} e^{\frac{-j2\pi\varepsilon T_C}{T_S}} e^{\frac{j2\pi(m+\varepsilon)\tau}{T_S}} \\
& \times \left[\sum_{l=0}^{l_0} \sum_{k=0}^{K} \alpha_{k,l} e^{\frac{-j2\pi m(T_l+\tau_{k,l}+\tau)}{T_S}} \left(e^{-j2\pi\varepsilon} e^{\frac{-j2\pi\varepsilon(T_l+\tau_{k,l}+\tau)}{T_S}} - 1 \right) \right. \\
& \left. + \sum_{l=l_0+1}^{L} \sum_{k=0}^{K} \alpha_{k,l} e^{\frac{-j2\pi m(T_l+\tau_{k,l}+\tau)}{T_S}} \left(e^{-j2\pi\varepsilon} - e^{\frac{-j2\pi\varepsilon(T_l+\tau_{k,l}+\tau)}{T_S}} \right) \right]
\end{aligned}
$$

is reprinted from Eq. (3.22).

In Subsection 3.3.2, we have seen that $\hat{c}_{m,i}^{ICI}$ and $\hat{c}_{m,i}^{ISI}$ are the sums of many independent but not identically distributed random variables. Thus we cannot apply the central limit theorem, which requires the sum of i.i.d. random variables, to model

the ICI and ISI as Gaussian random variables. However, to obtain performance bound, we will model the ICI and the ISI as Gaussian random variables whose mean is zeros and variance is σ_C^2 and σ_S^2, respectively, because independent Gaussian noise yields smallest capacity among additive noise processes with fixed variance and mean [6]. Consequently, z_m will be modelled as i.i.d. complex Gaussian random variable whose mean is zero and variance is

$$\sigma_Z^2 = \sigma_C^2 + \sigma_S^2 + N_0 \tag{3.58}$$

in which σ_C^2, σ_S^2, and N_0 are the variances of the ICI, the ISI, and the AWGN, respectively, and are quantified in Section 3.3.3.

Since the UWB system supports ten different data rates [8] that can be grouped into three different data-rate modes based on the overall spreading gain factor of 1, 2, or 4 obtained from OFDM modulation, we will consider the average probability of bit error for these three cases. As we have seen in Chapter 2, in the first case (with a gain factor of 1), each carrier frequency and time slot are used to transmit different information. In the second case (with a gain factor of 2), the same information is transmitted in two different time slots. In the third case (with a gain factor of 4), the same information is transmitted by using two frequency carriers and two time slots. These three cases share the same receiving model, i.e.,

$$\hat{\mathbf{c}} = c_{m,i}\mathbf{h} + \mathbf{z} \tag{3.59}$$

where $\hat{\mathbf{c}}$ is a vector comprising the demodulated signals $\hat{c}_{m,i}$, $\mathbf{h}$ is a vector consisting of the fading terms H_m associated with $\hat{c}_{m,i}$, and $\mathbf{z} \sim CN(0, \sigma_Z^2\mathbb{I})$, with the identical matrix $\mathbb{I}$, is the noise vector. Depending on different data-rate modes, $\hat{\mathbf{c}}$, $\mathbf{h}$, and $\mathbf{z}$

are different and will be classified later. These modes share the same detection rule, the maximum likelihood (ML) detection, in which the detected symbol

$$\tilde{c}_{m,i} = \underset{c_{m,i}}{\operatorname{argmin}} \|\hat{\mathbf{c}} - c_{m,i}\mathbf{h}\|^2. \tag{3.60}$$

The average probability of bit error for the three different cases cannot be determined directly but through the probability of symbol error [20]. Since the system employs QPSK modulation, $P_b = P_s$ where P_b and P_s are the probability of bit error and that of symbol error [20], respectively. Our main task now is to determine the probability of symbol error P_s.

The average probability of symbol error can be determined by averaging the probability of symbol error given the vector $\mathbf{h}$, a random vector due to its dependency to the random fading term H_m [20] [21]. That is that

$$P_s = E\left\{P_s(\mathbf{h})\right\}. \tag{3.61}$$

Based on the detection rule in Eq. (3.60), the probability of symbol error given the fading term is [21]

$$
\begin{aligned}
P_s(\mathbf{h}) &= \operatorname{Pr}\left[\|\hat{\mathbf{c}} - \tilde{c}_{m,i}\mathbf{h}\|^2 < \|\hat{\mathbf{c}} - c_{m,i}\mathbf{h}\|^2\right] \\
&= \operatorname{Pr}\left[\operatorname{Re}\left\{(c_{m,i} - \tilde{c}_{m,i})^*\mathbf{h}^H\mathbf{z}\right\} < -\frac{1}{2}|c_{m,i} - \tilde{c}_{m,i}|^2\|\mathbf{h}\|^2\right]
\end{aligned} \tag{3.62}
$$

where $\operatorname{Re}(x)$ yields the real component of the complex-valued x and $\|.\|$ represents the Frobenius-norm. Because $\mathbf{z} \sim CN(0, \sigma_Z^2\mathbb{I})$, $\operatorname{Re}\left\{(c_{m,i} - \tilde{c}_{m,i})^*\mathbf{h}^H\mathbf{z}\right\} \sim N\left(0, \frac{1}{2}|c_{m,i} - \tilde{c}_{m,i}|^2\|\mathbf{h}\|^2\sigma_Z^2\right)$. Thus simplifications yield

$$
\begin{aligned}
P_s(\mathbf{h}) &= \operatorname{Pr}\left[X < -\frac{|c_{m,i} - \tilde{c}_{m,i}|\|\mathbf{h}\|}{\sigma_Z\sqrt{2}}\right] \\
&= Q\left(\sqrt{2\rho}\right)
\end{aligned} \tag{3.63}
$$

56

where $X \sim N(0,1)$ and Q(.) represents the Q-function and is defined as [18] $Q(x) = \frac{1}{\sqrt{2\pi}} \int_x^\infty \exp(-\frac{t^2}{2})dt$. In Eq. (3.63), we have defined

$$\rho = \|\mathbf{h}\|^2 \frac{E_b}{\sigma_Z^2} \tag{3.64}$$

using the fact that the distance between QPSK symbols $|c_{m,i} - \tilde{c}_{m,i}|$ relates to the energy per bit E_b as $|c_{m,i} - \tilde{c}_{m,i}| = 2\sqrt{E_b}$. Our remaining task is to determine the PDF $f_\rho(t)$ for the three data-rate modes so that the average probability of symbol error can be determined as

$$P_s = \int_0^\infty f_\rho(t)Q(\sqrt{2t})dt. \tag{3.65}$$

Note that when ρ is a chi-square with $2m$ degrees of freedom random variable, its PDF is [20]:

$$f_\rho(t) = \frac{1}{(m-1)!(\overline{\gamma_\rho})^m} t^{m-1} e^{-t/\overline{\gamma_\rho}} \qquad \text{for } t \geq 0 \tag{3.66}$$

where $\overline{\gamma_\rho} \triangleq E\{\rho\}$ is the expectation of ρ corresponding to $m = 1$. Thus the average probability of symbol error is [20]

$$P_s = p^m \sum_{k=0}^{m-1} \binom{m-1+k}{k} (1-p)^k \tag{3.67}$$

where we have defined

$$p \triangleq \frac{1}{2}\left(1 - \sqrt{\frac{\overline{\gamma_\rho}}{1+\overline{\gamma_\rho}}}\right). \tag{3.68}$$

Next, following the approach presented in [14], we will demonstrate that approximately ρ has a chi-square distribution with $2m$ degrees of freedom, where m is the overall spreading gain factor.

A. The Case of Overall Spreading Gain Factor of 1

In this case, we do not have any diversity gain. Each frequency carrier and each time slot are used to transmit different information. The demodulated signal is

$$\hat{c}_{m,i} = c_{m,i} H_m + z. \tag{3.69}$$

Thus $\mathbf{h}$ is just the scalar H_m and

$$\rho = \frac{E_b}{\sigma_Z^2} \eta \tag{3.70}$$

where we have introduced $\eta = |H_m|^2$. From Eq. (3.22), we can rewrite the fading term as

$$H_m = \frac{1}{-j2\pi\varepsilon} e^{\frac{-j2\pi\varepsilon T_C}{T_S}} e^{\frac{j2\pi(m+\varepsilon)\tau}{T_S}} \mathbf{w}^H \mathbb{T} \, \mathbf{a} \tag{3.71}$$

where $\mathbf{w} = \left[\omega_m^{T_0+\tau_{0,0}+\tau}, \ \omega_m^{T_0+\tau_{0,1}+\tau}, \ ..., \ \omega_m^{T_L+\tau_{K,L}+\tau} \right]^T$, in which $\omega_m = \exp\left(\frac{-j2\pi m}{T_S}\right)$,

$\mathbb{T} = \mathrm{diag}\left(e^{-j2\pi\varepsilon} e^{\frac{-j2\pi\varepsilon(T_0+\tau_{0,0}+\tau)}{T_S}} - 1, \ ..., e^{-j2\pi\varepsilon} e^{\frac{-j2\pi\varepsilon(T_{l_0}+\tau_{K,l_0}+\tau)}{T_S}} - 1, \ e^{-j2\pi\varepsilon} \right.$

$\left. e^{\frac{-j2\pi\varepsilon(T_{l_0+1}+\tau_{0,l_0+1}+\tau)}{T_S}} - 1, \ ..., e^{-j2\pi\varepsilon} e^{\frac{-j2\pi\varepsilon(T_L+\tau_{K,L}+\tau)}{T_S}} - 1 \right)$ and $\mathbf{a} = \left[\alpha_{0,0}, \ \alpha_{0,1}, \ ..., \right.$

$\left. \alpha_{K,L} \right]^T$. Because $\alpha_{k,l} \sim CN(0, \Omega_{k,l})$ where $\Omega_{k,l}$ follows Eq. (3.4) in Section 3.2, we can rewrite $\mathbf{a} = \boldsymbol{\Omega}^{\frac{1}{2}} \mathbf{b}$ where $\boldsymbol{\Omega}^{\frac{1}{2}} \, \boldsymbol{\Omega}^{\frac{1}{2}} = \boldsymbol{\Omega} = \mathrm{diag}\left(\Omega_{0,0}, \ \Omega_{0,1}, \ ..., \ \Omega_{K,L} \right)$ and $\mathbf{b} = \left[\beta'_{0,0}, \ \beta'_{0,1}, \ ..., \ \beta'_{K,L} \right]^T$ where $\beta'_{k,l} \sim CN(0, 1)$. Hence

$$H_m = \frac{1}{-j2\pi\varepsilon} e^{\frac{-j2\pi\varepsilon T_C}{T_S}} e^{\frac{j2\pi(m+\varepsilon)\tau}{T_S}} \mathbf{w}^H \mathbb{T} \, \boldsymbol{\Omega}^{\frac{1}{2}} \mathbf{b} \tag{3.72}$$

and consequently,

$$\eta = \frac{1}{4\pi^2\varepsilon^2} \mathbf{b}^H \boldsymbol{\Omega}^{\frac{1}{2}} \mathbb{T} \mathbf{w} \mathbf{w}^H \mathbb{T} \boldsymbol{\Omega}^{\frac{1}{2}} \mathbf{b}. \tag{3.73}$$

Let us define $\boldsymbol{\Psi} = \boldsymbol{\Omega}^{\frac{1}{2}} \mathbb{T} \mathbf{w} \mathbf{w}^H \mathbb{T} \boldsymbol{\Omega}^{\frac{1}{2}}$. Clearly, $\boldsymbol{\Psi}$ is a non-negative definite Hermitian matrix. Based on the singular-value decomposition theorem [22], we can

express

$$\boldsymbol{\Psi} = \mathbb{V}\boldsymbol{\Lambda}\mathbb{V}^H \tag{3.74}$$

where $\boldsymbol{\Lambda}$ is a diagonal matrix containing the real and non-negative eigenvalues of $\boldsymbol{\Psi}$ and $\mathbb{V}$ is a unitary matrix containing the eigenvectors associating with the eigenvalues in $\boldsymbol{\Lambda}$. Since $\mathrm{rank}(\boldsymbol{\Psi}) \leq \min\{\mathrm{rank}(\boldsymbol{\Omega}^{\frac{1}{2}}), \mathrm{rank}(\mathbb{T}), \mathrm{rank}(\mathbf{w})\}$ where $\mathrm{rank}(\boldsymbol{\Omega}^{\frac{1}{2}}) = \mathrm{rank}(\mathbb{T}) = (K+1)(L+1)$ and $\mathrm{rank}(\mathbf{w}) = 1$, there exists only one nonzero eigenvalue in $\boldsymbol{\Lambda}$. Thus the eigenvalue is evaluated as

$$
\begin{aligned}
\mathrm{eig}(\boldsymbol{\Psi}) &= \mathrm{eig}(\mathbf{w}^H \mathbb{T}\boldsymbol{\Omega}\mathbb{T}\mathbf{w}) \\
&= \sum_{l=0}^{l_0}\sum_{k=0}^{K}\Omega_{k,l}\left[2 - \left(e^{-j2\pi\varepsilon}e^{\frac{-j2\pi\varepsilon(T_l+\tau_{k,l}+\tau)}{T_S}} + e^{j2\pi\varepsilon}e^{\frac{j2\pi\varepsilon(T_l+\tau_{k,l}+\tau)}{T_S}}\right)\right] \\
&\quad + \sum_{l=l_0+1}^{L}\sum_{k=0}^{K}\Omega_{k,l}\left[2 - \left(e^{-j2\pi\varepsilon}e^{\frac{j2\pi\varepsilon(T_l+\tau_{k,l}+\tau)}{T_S}} + e^{j2\pi\varepsilon}e^{\frac{-j2\pi\varepsilon(T_l+\tau_{k,l}+\tau)}{T_S}}\right)\right].
\end{aligned}
$$

Consequently, we obtain

$$
\begin{aligned}
\eta &= \frac{1}{4\pi^2\varepsilon^2}\left(\sum_{l=0}^{l_0}\sum_{k=0}^{K}\Omega_{0,0}e^{-\frac{T_l}{\Gamma}-\frac{\tau_{k,l}}{\gamma}}\right. \\
&\quad \times \left[2 - \left(e^{-j2\pi\varepsilon}e^{\frac{-j2\pi\varepsilon(T_l+\tau_{k,l}+\tau)}{T_S}} + e^{j2\pi\varepsilon}e^{\frac{j2\pi\varepsilon(T_l+\tau_{k,l}+\tau)}{T_S}}\right)\right] \\
&\quad + \sum_{l=l_0+1}^{L}\sum_{k=0}^{K}\Omega_{0,0}e^{-\frac{T_l}{\Gamma}-\frac{\tau_{k,l}}{\gamma}} \\
&\quad \left. \times \left[2 - \left(e^{-j2\pi\varepsilon}e^{\frac{j2\pi\varepsilon(T_l+\tau_{k,l}+\tau)}{T_S}} + e^{j2\pi\varepsilon}e^{\frac{-j2\pi\varepsilon(T_l+\tau_{k,l}+\tau)}{T_S}}\right)\right]\right)|\beta|^2
\end{aligned}
$$

where $\beta \sim CN(0,1)$ and we have substituted $\Omega_{k,l}$ by the expression in Eq. (3.4).

Eq. (3.75) reveals that η is not a chi-square random variable with two degrees of freedom as in the case of Rayleigh fading channel described in [20] and [21]. Here η is a product of a chi-square random variable $|\beta|^2$ and another random variable that is the sum of many combinations of the $k-$ and $l-$Erlang random variables T_l

and $\tau_{k,l}$. Therefore, finding the PDF of η, and hence of ρ is a difficult task, if not impossible.

To be able to solve the problem, we will employ the approximation approach in [14]. From Eq. (3.64), η is in a quadratic form. Using a representation of quadratic form in [23], and noting that $E\{\mathbf{h}\} = 0$, we can approximate η by

$$\eta \approx \sum_{s=1}^{S} \text{eig}_s(\mathbf{\Phi})|\mu_s|^2 \tag{3.75}$$

where $\mu_s \sim CN(0,1)$ and S is the rank of matrix $\mathbf{\Phi}$ defined as

$$\mathbf{\Phi} = E\left\{\mathbf{h}\mathbf{h}^H\right\}. \tag{3.76}$$

For the case of the gain factor of 1, $\mathbf{h} = H_m$, thus $\mathbf{\Phi} = \sigma_H^2$, the variance of the fading term. Combining all together provides

$$\rho \approx \frac{E_b \sigma_H^2}{\sigma_Z^2}|\mu|^2. \tag{3.77}$$

Since $\mu \sim CN(0,1)$, $|\mu|^2$ has a chi-square probability distribution with two degrees of freedom. Consequently, ρ approximately is chi-square-distributed with two degrees of freedom, as shown in Eq. (3.77). The expectation of ρ is

$$\begin{aligned}
\overline{\gamma_\rho} &= \frac{E_b \sigma_H^2}{\sigma_Z^2} \\
&= \frac{\sigma_H^2}{2\tilde{\sigma}_C^2 + 2\tilde{\sigma}_S^2 + \frac{N_0}{E_b}} \\
&= \overline{\gamma_b}(\varepsilon, \tau) \tag{3.78}
\end{aligned}$$

where $\overline{\gamma_b}(\varepsilon, \tau)$ is the average SNR per bit, defined in Eq. (3.54). Note that in Eq. (3.78), we have substituted σ_Z^2 by the expression in Eq. (3.58) and used the fact that $E_b = \frac{1}{2}E_s$.

60

Based on Eq. (3.67) with $m = 1$ and Eq. (3.68), the average probability of symbol error, and hence of bit error for this case is

$$P_b = P_s \approx \frac{1}{2} \left(1 - \sqrt{\frac{\overline{\gamma_b}(\varepsilon, \tau)}{1 + \overline{\gamma_b}(\varepsilon, \tau)}} \right). \tag{3.79}$$

B. The Case of Overall Spreading Gain Factor of 2

In this case, we obtain the time diversity gain by transmitting the same information in two consecutive time slots. At the receiver, the following two received signals containing the transmitted symbol $c_{m,i}$

$$
\begin{aligned}
\hat{c}_{m,i} &= c_{m,i} H_{m,i} + z \\
\hat{c}_{m,i+1} &= c_{m,i} H_{m,i+1} + z.
\end{aligned} \tag{3.80}
$$

Here we assume that the fading terms $H_{m,i}$ and $H_{m,i+1}$ are i.i.d., denoted as H_m^1 and H_m^2 with mean zero and variance σ_H^2 because they share the same subcarrier index m. Hence the fading-term vector in Eq. (3.60) is just $\mathbf{h} = [H_m^1 \ H_m^2]^T$ and the noise vector $\mathbf{z} \sim CN(0, \sigma_Z^2 \mathbb{I}_2)$ with $\mathbb{I}$ denoting the identity matrix. Thus

$$\rho = \frac{E_b}{\sigma_Z^2} \eta \tag{3.81}$$

where we have introduced $\eta = \|\mathbf{h}\|^2 = |H_m^1|^2 + |H_m^2|^2$. Following the procedure in **A**, we can show that

$$
\begin{aligned}
\eta = \ &\frac{1}{4\pi^2 \varepsilon^2} \left(\sum_{l=0}^{l_0} \sum_{k=0}^{K} \Omega_{0,0} e^{-\frac{T_l}{\Gamma} - \frac{\tau_{k,l}}{\gamma}} \right. \\
&\times \left. \left[2 - \left(e^{-j2\pi\varepsilon} e^{\frac{-j2\pi\varepsilon(T_l + \tau_{k,l} + \tau)}{T_S}} + e^{j2\pi\varepsilon} e^{\frac{j2\pi\varepsilon(T_l + \tau_{k,l} + \tau)}{T_S}} \right) \right] \right)
\end{aligned}
$$

61

$$+ \sum_{l=l_0+1}^{L} \sum_{k=0}^{K} \Omega_{0,0} e^{-\frac{T_l}{\Gamma} - \frac{\tau_{k,l}}{\gamma}}$$

$$\times \left[2 - \left(e^{-j2\pi\varepsilon} e^{\frac{j2\pi\varepsilon(T_l+\tau_{k,l}+\tau)}{T_S}} + e^{j2\pi\varepsilon} e^{\frac{-j2\pi\varepsilon(T_l+\tau_{k,l}+\tau)}{T_S}} \right) \right] \Big)$$

$$\times (|\beta_1|^2 + |\beta_2|^2) \tag{3.82}$$

where $\beta_{1,2} \sim CN(0,1)$. Eq. (3.82) reveals that η in this case relates to, but not exactly, a chi-square random variable with four degrees of freedom. Thus the PDF of η is difficult to find, if not impossible.

To derive the PDF of η, we again follow the approximation approach presented in **A**. In this approach, η is first approximated as

$$\eta \approx \sum_{s=1}^{S} \text{eig}_s(\mathbf{\Phi}) |\mu_s|^2 \tag{3.83}$$

where $\mu_s \sim CN(0,1)$ and S is the rank of matrix $\mathbf{\Phi}$ defined as

$$\begin{aligned}
\mathbf{\Phi} &= E\left\{ \mathbf{h}\mathbf{h}^H \right\} \\
&= \begin{pmatrix} \sigma_H^2 & 0 \\ 0 & \sigma_H^2 \end{pmatrix}
\end{aligned} \tag{3.84}$$

since H_m^1 and H_m^2 are i.i.d.. Clearly, $\mathbf{\Phi}$ has two eigenvalues $\text{eig}_1(\mathbf{\Phi}) = \text{eig}_2(\mathbf{\Phi}) = \sigma_H^2$. Combining all together provides

$$\rho \approx \frac{E_b \sigma_H^2}{\sigma_Z^2} \left(|\mu_1|^2 + |\mu_2|^2 \right) \tag{3.85}$$

where $\mu_{1,2} \sim CN(0,1)$. Eq. (3.85) reveals that the random variable ρ approximately has a chi-square distribution with four degrees of freedom. Based on Eq. (3.67) with $m=2$ and Eq. (3.68), the average probability of symbol error, and hence of bit error for this case is

$$P_b = P_s \approx p^2(3-2p) \tag{3.86}$$

where p is defined in Eq. (3.68) with $\overline{\gamma_\rho} = \overline{\gamma_b}(\varepsilon, \tau)$.

C. The Case of Overall Spreading Gain Factor of 4

In this case, we obtain both frequency and time diversity gain by transmitting the same information using two frequency carriers and two consecutive time slots. At the receiver, the following four received signals contain the transmitted symbol $c_{m,i}$

$$
\begin{aligned}
\hat{c}_{m,i} &= c_{m,i} H_m + z \\
\hat{c}_{m,i+1} &= c_{m,i} H_m + z \\
\hat{c}_{N-m-1,i} &= c^*_{m,i} H_{N-m-1} + z \\
\hat{c}_{N-m-1,i+1} &= c^*_{m,i} H_{N-m-1} + z
\end{aligned}
\tag{3.87}
$$

where * denotes the complex conjugate. We can rewrite Eq. (3.87) as

$$
\hat{\mathbf{c}} = c_{m,i} \mathbf{h} + \mathbf{z}
\tag{3.88}
$$

where $\hat{\mathbf{c}} = \begin{bmatrix} \hat{c}_{m,i} \ \hat{c}_{m,i+1} \ \hat{c}^*_{N-m-1,i} \ \hat{c}^*_{N-m-1,i+1} \end{bmatrix}^T$, $\mathbf{h} = \begin{bmatrix} H_m \ H_m \ H^*_{N-m-1} \ H^*_{N-m-1} \end{bmatrix}^T$ and $\mathbf{z} \sim CN(0, \sigma_Z^2 \mathbb{I}_4)$. Thus

$$
\rho = \frac{E_b}{\sigma_Z^2} \eta
\tag{3.89}
$$

where we have introduced $\eta = \|\mathbf{h}\|^2 = |H_m^1|^2 + |H_m^2|^2 + |H_{N-m-1}^1|^2 + |H_{N-m-1}^2|^2$. Notice that H_m and H_{N-m-1} are not independent since they belong to different subchannels. Following the procedure in **A**, we can show that

$$
\eta = \frac{1}{4\pi^2 \varepsilon^2} \left(\sum_{l=0}^{l_0} \sum_{k=0}^{K} \Omega_{0,0} e^{-\frac{T_l}{\Gamma} - \frac{\tau_{k,l}}{\gamma}} \right.
$$

$$\times \left[2 - \left(e^{-j2\pi\varepsilon} e^{\frac{-j2\pi\varepsilon(T_l + \tau_{k,l} + \tau)}{T_S}} + e^{j2\pi\varepsilon} e^{\frac{j2\pi\varepsilon(T_l + \tau_{k,l} + \tau)}{T_S}} \right) \right]$$

$$+ \sum_{l=l_0+1}^{L} \sum_{k=0}^{K} \Omega_{0,0} e^{-\frac{T_l}{\Gamma} - \frac{\tau_{k,l}}{\gamma}}$$

$$\times \left[2 - \left(e^{-j2\pi\varepsilon} e^{\frac{j2\pi\varepsilon(T_l + \tau_{k,l} + \tau)}{T_S}} + e^{j2\pi\varepsilon} e^{\frac{-j2\pi\varepsilon(T_l + \tau_{k,l} + \tau)}{T_S}} \right) \right] \bigg)$$

$$\times (|\beta_1|^2 + |\beta_2|^2 + |\beta_3|^2 + |\beta_4|^2) \tag{3.90}$$

where $\beta_x \sim CN(0,1)$ for $x = 1$, 2, 3, or 4. Eq. (3.90) reveals that η in this case relates to, but not exactly, a chi-square random variable with eight degrees of freedom. The PDF of η is difficult to find, if not impossible.

To derive the PDF of η, we again follow the approximation approach presented in **A**. In this approach, η is first approximated as

$$\eta \approx \sum_{s=1}^{S} \text{eig}_s(\mathbf{\Phi})|\mu_s|^2 \tag{3.91}$$

where $\mu_s \sim CN(0,1)$ and S is the rank of matrix $\mathbf{\Phi}$ defined as

$$\mathbf{\Phi} \triangleq E\left\{ \mathbf{h}\mathbf{h}^H \right\}$$

$$= \begin{pmatrix} \sigma_H^2 & 0 & R_{(N-m-1),m} & R_{(N-m-1),m} \\ 0 & \sigma_H^2 & R_{(N-m-1),m} & R_{(N-m-1),m} \\ R_{(N-m-1),m}^* & R_{(N-m-1),m}^* & \sigma_H^2 & 0 \\ R_{(N-m-1),m}^* & R_{(N-m-1),m}^* & 0 & \sigma_H^2 \end{pmatrix}$$

where $R_{(N-m-1),m} = E\left\{ H_m H_{N-m-1} \right\}$ is the complementary correlation between the fading terms at subcarrier m and its symmetric conjugate at subcarrier $N - m - 1$. From the expression of H_m in Eq. (3.22) and using the fact that the multipath gain

coefficients $\alpha_{k,l}$ are statistically independent,

$$
\begin{aligned}
R_{(N-m-1),m} &= \frac{1}{4\pi^2\varepsilon^2} \sum_{l=0}^{l_0} \sum_{k=0}^{K} E\left\{ \Omega_{0,0} e^{-\frac{T_l}{\Gamma}-\frac{\tau_{k,l}}{\gamma}} e^{\frac{-j2\pi(N-1)(T_l+\tau_{k,l}+\tau)}{T_S}} \right. \\
&\quad \left. \times \left[2 - \left(e^{-j2\pi\varepsilon} e^{\frac{-j2\pi\varepsilon(T_l+\tau_{k,l}+\tau)}{T_S}} + e^{j2\pi\varepsilon} e^{\frac{j2\pi\varepsilon(T_l+\tau_{k,l}+\tau)}{T_S}} \right) \right] \right\} \\
&\quad + \frac{1}{4\pi^2\varepsilon^2} \sum_{l=l_0+1}^{L} \sum_{k=0}^{K} E\left\{ \Omega_{0,0} e^{-\frac{T_l}{\Gamma}-\frac{\tau_{k,l}}{\gamma}} e^{\frac{-j2\pi(N-1)(T_l+\tau_{k,l}+\tau)}{T_S}} \right. \\
&\quad \left. \times \left[2 - \left(e^{-j2\pi\varepsilon} e^{\frac{j2\pi\varepsilon(T_l+\tau_{k,l}+\tau)}{T_S}} + e^{j2\pi\varepsilon} e^{\frac{-j2\pi\varepsilon(T_l+\tau_{k,l}+\tau)}{T_S}} \right) \right] \right\} \\
&\triangleq R(N-1)
\end{aligned}
\tag{3.92}
$$

where we have used the fact that $N - m - 1 + m = N - 1$ and conditioned on T_l and $\tau_{k,l}$ to obtain the expression. Eq. (3.92) reveals that by placing the transmitted symbol $c_{m,i}$ in the symmetric conjugate positions to explore the frequency diversity, we have made these positions as less correlated as possible. Now if we define Γ' and γ' such that $\frac{1}{\Gamma'} = \frac{1}{\Gamma} + \frac{j2\pi(N-1)}{T_S}$ and $\frac{1}{\gamma'} = \frac{1}{\gamma} + \frac{j2\pi(N-1)}{T_S}$, then

$$
\begin{aligned}
R(N-1) &= \frac{1}{4\pi^2\varepsilon^2} e^{\frac{-j2\pi(N-1)\tau}{T_S}} \sum_{l=0}^{l_0} \sum_{k=0}^{K} E\left\{ \Omega_{0,0} e^{-\frac{T_l}{\Gamma'}-\frac{\tau_{k,l}}{\gamma'}} \right. \\
&\quad \left. \times \left[2 - \left(e^{-j2\pi\varepsilon} e^{\frac{-j2\pi\varepsilon(T_l+\tau_{k,l}+\tau)}{T_S}} + e^{j2\pi\varepsilon} e^{\frac{j2\pi\varepsilon(T_l+\tau_{k,l}+\tau)}{T_S}} \right) \right] \right\} \\
&\quad + \frac{1}{4\pi^2\varepsilon^2} e^{\frac{-j2\pi(N-1)\tau}{T_S}} \sum_{l=l_0+1}^{L} \sum_{k=0}^{K} E\left\{ \Omega_{0,0} e^{-\frac{T_l}{\Gamma'}-\frac{\tau_{k,l}}{\gamma'}} \right. \\
&\quad \left. \times \left[2 - \left(e^{-j2\pi\varepsilon} e^{\frac{j2\pi\varepsilon(T_l+\tau_{k,l}+\tau)}{T_S}} + e^{j2\pi\varepsilon} e^{\frac{-j2\pi\varepsilon(T_l+\tau_{k,l}+\tau)}{T_S}} \right) \right] \right\}
\end{aligned}
\tag{3.93}
$$

Comparing Eq. (3.93) with Eq. (3.31), we see that they are about identical. If we replace Γ and γ by Γ' and γ' in Eq. (3.31) and multiply the equation by $e^{\frac{-j2\pi(N-1)\tau}{T_S}}$, we obtain $R(N-1)$. Therefore, $R(N-1)$ can be expressed in term of the quantities $A_1(.)$, $A_2(.)$, $B_1(.)$, and $B_2(.)$, derived in Subsection 3.3.3. Particularly for the four considering cases of frequency and timing synchronization, we have

1. **Perfect frequency and timing synchronization, i.e., $\varepsilon = 0$ and $\tau = 0$:**

$$
\begin{aligned}
R(N-1) &= e^{\frac{-j2\pi(N-1)\tau}{T_S}} \left(\Omega_{0,0} + \frac{1}{T_S^2} A_2(T_S, 0, \lambda, \gamma') \right. \\
&\quad \left. + \frac{1}{T_S^2} A_2(T_S, 0, \Lambda, \Gamma') + \frac{1}{T_S^2} A_1(T_S, 0, \Lambda, \Gamma', \lambda, \gamma') \right)
\end{aligned}
$$

2. **Imperfect timing synchronization, i.e., $\varepsilon = 0$ and $\tau \neq 0$:**

$$
\begin{aligned}
R(N-1) &= e^{\frac{-j2\pi(N-1)\tau}{T_S}} \left(\Omega_{0,0} \frac{(\tau + T_S)^2}{T_S^2} + \frac{1}{T_S^2} A_2(-T_S - \tau, 0, \lambda, \gamma') \right. \\
&\quad + \frac{1}{T_S^2} A_2(-T_S - \tau, 0, \Lambda, \Gamma') - \frac{1}{T_S^2} A_2(-T_S - \tau, l_0, \Lambda, \Gamma') \\
&\quad + \frac{1}{T_S^2} A_2(T_S - \tau, l_0, \Lambda, \Gamma') + \frac{1}{T_S^2} A_1(-T_S - \tau, 0, \Lambda, \Gamma', \lambda, \gamma') \\
&\quad \left. - \frac{1}{T_S^2} A_1(-T_S - \tau, l_0, \Lambda, \Gamma', \lambda, \gamma') + \frac{1}{T_S^2} A_1(T_S - \tau, l_0, \Lambda, \Gamma', \lambda, \gamma') \right)
\end{aligned}
$$

3. **Imperfect frequency synchronization, i.e., $\varepsilon \neq 0$ and $\tau = 0$:**

$$
\begin{aligned}
R(N-1) &= \frac{1}{4\pi^2\varepsilon^2} e^{\frac{-j2\pi(N-1)\tau}{T_S}} \left[2\Omega_{0,0} \left(1 - \cos 2\pi\varepsilon \right) + B_2(0, 0, 0, \varepsilon, \varepsilon, 0, \lambda, \gamma') \right. \\
&\quad \left. + B_2(0, 0, 0, \varepsilon, \varepsilon, 0, \Lambda, \Gamma') + B_1(0, 0, 0, \varepsilon, \varepsilon, 0, \Lambda, \Gamma', \lambda, \gamma') \right]
\end{aligned}
$$

4. **Imperfect frequency and timing synchronization, i.e., $\varepsilon \neq 0$ and $\tau \neq 0$:**

$$
\begin{aligned}
R(N-1) &= \frac{1}{4\pi^2\varepsilon^2} e^{\frac{-j2\pi(N-1)\tau}{T_S}} \left[2\Omega_{0,0} \left(1 - \cos\left(\frac{2\pi\varepsilon\tau}{T_S} + 2\pi\varepsilon \right) \right) \right. \\
&\quad + B_2(-\tau, 0, 0, \varepsilon, -\varepsilon, 0, \lambda, \gamma') + B_2(-\tau, 0, 0, \varepsilon, -\varepsilon, 0, \Lambda, \Gamma') \\
&\quad - B_2(-\tau, 0, 0, \varepsilon, -\varepsilon, l_0, \Lambda, \Gamma') + B_2(-\tau, 0, 0, \varepsilon, \varepsilon, l_0, \Lambda, \Gamma') \\
&\quad + B_1(-\tau, 0, 0, \varepsilon, -\varepsilon, 0, \Lambda, \Gamma', \lambda, \gamma') - B_1(-\tau, 0, 0, \varepsilon, -\varepsilon, l_0, \Lambda, \Gamma', \lambda, \gamma') \\
&\quad \left. + B_1(-\tau, 0, 0, \varepsilon, \varepsilon, l_0, \Lambda, \Gamma', \lambda, \gamma') \right]
\end{aligned}
$$

Note that when we use the $R(N-1)$ expressions, we need to pay attention to Remarks 6-11 in Subsection 3.3.3.

Let us define $r \triangleq \frac{R(N-1)}{\sigma_H^2}$: the normalized complementary correlation between the fading terms at subcarrier m and its symmetric conjugate at subcarrier $N-m-1$. Then

$$\mathbf{\Phi} = \sigma_H^2 \begin{pmatrix} 1 & 0 & r & r \\ 0 & 1 & r & r \\ r^* & r^* & 1 & 0 \\ r^* & r^* & 0 & 1 \end{pmatrix} \tag{3.94}$$

whose eigenvalues can be shown as

$$\text{eig}(\mathbf{\Phi}) = \sigma_H^2 \left[1 + |r|, \ 1, \ 1, \ 1 - |r| \right]^T \tag{3.95}$$

Combining all together, we obtain the interested random variable ρ in Eq. (3.89) as

$$\rho \approx \frac{E_b \sigma_H^2}{\sigma_Z^2} \left((1 + |r|)|\mu_1|^2 + |\mu_2|^2 + |\mu_3|^2 + (1 - |r|)|\mu_4|^2 \right) \tag{3.96}$$

Based on Eq. (3.96), the probability of symbol error will be determined in the following two cases.

1. When $|r| \ll 1$, ρ approximately is a chi-square random variable with eight degrees of freedom. Based on Eq. (3.67) with $m = 4$ and Eq. (3.68), the average probability of symbol error, and hence of bit error for this case is

$$P_b = P_s \approx p^4 \sum_{k=0}^{3} \binom{3+k}{k} (1-p)^k \tag{3.97}$$

where p is defined in Eq. (3.68) with $\overline{\gamma_\rho} = \overline{\gamma_b}(\varepsilon, \tau)$.

67

2. When we cannot ignore r, ρ is no longer chi-square-distributed because it is not a sum of i.i.d. random variables. This reflects the fact that the fading in different subchannels are correlated to each other. To find the average probability of symbol error, we will follow the approach in [14]. Using the alternative representation of the Q-function [24], $Q(x) = \frac{1}{\pi} \int_0^{\pi/2} \exp\left(-\frac{x^2}{2\sin^2\theta}\right) d\theta$ for $x \geq 0$, the average probability of symbol error can be expressed as

$$P_s = \frac{1}{\pi} \int_0^{\pi/2} M_\rho\left(-\frac{1}{\sin^2\theta}\right) d\theta \tag{3.98}$$

where $M_\rho(s) = E\{e^{s\rho}\}$ is the MGF of ρ. Because ρ is the sum of independent chi-square random variables, its MGF can be shown as

$$M_\rho(s) \approx \frac{1}{\left(1 - s\overline{\gamma_\rho}(1 + |r|)\right)\left(1 - s\overline{\gamma_\rho}\right)^2\left(1 - s\overline{\gamma_\rho}(1 - |r|)\right)} \tag{3.99}$$

where $\overline{\gamma_\rho} = \overline{\gamma_b}(\varepsilon, \tau)$. Consequently, the average probability of symbol error, and hence of bit error is

$$P_b = P_s \approx \frac{1}{\pi} \int_0^{\pi/2} \frac{\sin^8\theta}{\left(\sin^2\theta + \overline{\gamma_\rho}(1 + |r|)\right)\left(\sin^2\theta + \overline{\gamma_\rho}\right)^2\left(\sin^2\theta + \overline{\gamma_\rho}(1 - |r|)\right)} d\theta \tag{3.100}$$

For our OFDM UWB system, the average bit error probability for the high-rate mode can follow Eq. (3.97) since the normalized complementary correlation r is relatively small. For example, in the case of perfect frequency and timing synchronization, $r = 0.0987$, 0.0141, 0.0018, and 7.8343^{-004}, computed for CM1, CM2, CM3, and CM4 respectively. Figure 3.4 shows the average bit error probability for the perfect synchronization case in CM1, CM2, CM3, and CM4. The probability is plotted using Eq. (3.100) in the solid curve (denoted as Exact) and using Eq.
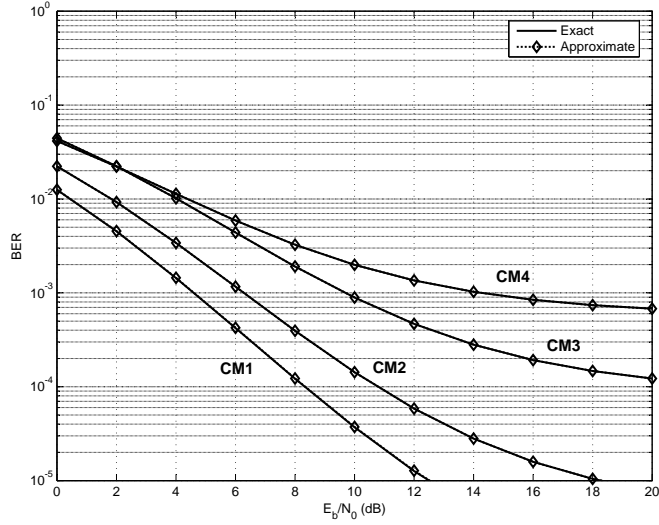
Figure 3.4: **The average bit error probability of the OFDM system for the high data rate mode in channel model CM1.**

(3.97) in the dotted-diamond curve (denoted as Approximate). Clearly, the curves match each other very well, and thus we can use the approximation for our case.

We have completely derived the average probability of bit error for the OFDM system. Depending on the data rate modes: high rate, middle rate, or low rate, the average bit error probability will follow Eq. (3.79), Eq. (3.86), or Eqs. (3.97) or (3.100) (depending on the value of the normalized complementary correlation r). The numerical and simulated results of the average probability will be presented and analyzed in Section 3.5. In the next section, we will outline the way to obtain the performance bound of the entire MB-OFDM UWB system.

3.4 The Performance Bound of the Entire MB-OFDM UWB System

Now we will consider the performance of the entire MB-OFDM UWB system, i.e., including the convolutional encoder and bit-interleaver at the transmitter and the Viterbi decoder and the bit-deinterleaver at the receiver. As shown in Figure 3.1, a transmitted binary sequence is input into the channel encoder. Redundancy is added to the sequence to improve the SNR for a better detection at the receiver. For our MB-OFDM UWB system, this process is done through the convolutional coding and puncturing. The bit-interleaver is used to prevent burst errors. After that, the binary sequence is modulated in the OFDM modulation and transmitted through the multipath fading channel with AWGN. At the receiver, after the OFDM demodulation, we obtain a binary sequence with a certain bit error probability. The average bit error probability is determined as in previous section. This binary sequence is input into the bit-deinterleaver to obtain an output sequence, which is then filled with dummy "zero" metrics in the de-puncturing process. After that, hard-decision Viterbi decoding is applied to obtain the received binary sequence.

The bit error probability for the entire system can be bounded as [21]

$$P_b^s \leq \frac{1}{M} \sum_{d=d_{free}}^{\infty} \beta_d P_d \qquad (3.101)$$

where M is the puncturing period, d_{free} is the free distance of the channel code, β_d is the weight spectrum representing the number of paths corresponding to the distance d, and P_d is the probability of selecting the incorrect path at distance d

and can be determined as

$$P_d = \begin{cases} \sum_{k=(d+1)/2}^{d} \binom{d}{k} P_b^k (1 - P_b)^{d-k} & d \text{ odd} \\ \frac{1}{2} \binom{d}{d/2} P_b^{d/2} (1 - P_b)^{d/2} + \sum_{k=d/2+1}^{d} \binom{d}{k} P_b^k (1 - P_b)^{d-k} & d \text{ even} \end{cases} \quad (3.102)$$

where

$$P_b = \int_0^{\infty} f_\rho(t) Q(\sqrt{2t}) dt \qquad (3.103)$$

is the average probability of bit error after the OFDM demodulation block. The remaining task is how to find the weight spectrum β_d corresponding to the convolutional code and the puncturing patterns in the system. Theoretically, β_d can be found based on the transfer function of the convolutional code [21]. The transfer function is obtained through solving the state equations. However, it is practically difficult to find the transfer function, especially for the convolutional code with large constraint length. For the mother code with coding rate $R = 1/3$ in our system, there are a total of 64 states. Thus we need to derive and solve symbolically a linear system of 64 state equations for the transfer function. This is a difficult task. For the puncture codes in our system, obtaining the transfer functions is impossible. An alternative approach is to use computers to search for the free distance d_{free} and the weight spectrum β_d, for example, as being done in [25]. However, that is not our main focus in this thesis. If the information of d_{free} and β_d is available, following Eq. (3.101) should provide us the performance bound of the entire MB-OFDM UWB system.

3.5 Numerical and Simulated Results

In this section, the degradation ratio and the average bit error probability of the OFDM system will be evaluated based on Eqs. (3.55), (3.79), (3.86), (3.97), and (3.100) in Subsection 3.3.5. The four UWB channel models: CM1, CM2, CM3, and CM4 and various conditions of frequency and timing synchronization will be considered. Particularly, we choose to present the average bit error probability of the system in the cases of perfect frequency and timing synchronization and of imperfect timing synchronization. In addition, we will also present the system performance degradation through the degradation ratio in the cases of imperfect frequency synchronization and of imperfect frequency and timing synchronization.

The OFDM system has $N = 128$ subcarriers and the subband bandwidth of 528 MHz. The durations of the useful OFDM symbol, the cyclic prefix, and the guard interval are $T_S = 242.42$ nsec, $T_C = 60.61$ nsec, and $T_G = 9.47$ nsec, respectively. The total symbol duration is $T'_S = 312.5$ nsec. The arrival rates Λ and λ and the decay factors Γ and γ of the cluster and ray, respectively, follow Table 3.1. In Subsection 3.5.1, the numerical result will be presented and analyzed. The simulated result will be presented in Subsection 3.5.2.

3.5.1 Numerical Results

In Figure 3.5, we plot the average bit error probability BER versus SNR per bit E_b/N_0 of the OFDM system in the perfect frequency and timing synchronization in the four channel models. Two conclusions can be drawn from the figure. First,

Figure 3.5: **The average probability of bit error of the OFDM system in perfect frequency and timing synchronization in different UWB channel models: (a) CM1; (b) CM2; (c) CM3; and (d) CM4.**

as the data rate increases, at the same SNR, the average bit error probability also increases. This is due to the spreading gain the data rate mode inherits. The higher the spreading gain factor is the more diversity order, and hence the lower the average bit error probability. As we have seen in Chapter 2, the low-rate mode, consisting data rates of 80 Mbps or less, has the largest spreading gain factor of 4, and thus it has the lowest average probability of bit error as shown in Figure 3.5. On the other hands, the high-rate mode, comprising data rate of 320 Mbps or higher, has

spreading gain factor of 1 (no diversity gain), and thus it has the largest average bit error probability. The middle-rate mode lies in between of these other two data-rate modes since it inherits a spreading gain factor of 2.

The second conclusion from the figure is that as the severity of the channel increases, the average bit error probability also increases. This is obvious in the figure. Among these channel models, CM1 is the least severe and has the lowest average bit error probability while CM4 is the most severe and results in the highest average bit error probability, when compared at the same SNR.

In Figure 3.6, we plot the average bit error probability of the OFDM system against the SNR per bit in different relative timing synchronization error, defined as $\delta\tau \triangleq \frac{\tau}{T_S}$, to illustrate the OFDM system performance in the imperfect timing synchronization. Again, two conclusions can be drawn from the figure. First, the positive timing errors always make the performance become worse while small negative timing errors can improve the system performance. As we have presented in Subsection 3.3.1, positive timing error corresponds to the misplacement of the FFT window into the current OFDM symbol (See Figure 3.3(a)). Equivalently, we have the perfect timing synchronization but the received signal arrives with an extra delay τ. Therefore, the current OFDM symbol receives more ISI from the previous OFDM symbol, and that worsens the system performance. On the other hands, the small negative timing error is equivalent to the reduction of the channel delays, and thus improves the system performance. Note that the negative timing error places the current OFDM symbol into the cyclic prefix region of the next OFDM symbol, and thus could cause the current symbol to receive the ISI from the next OFDM
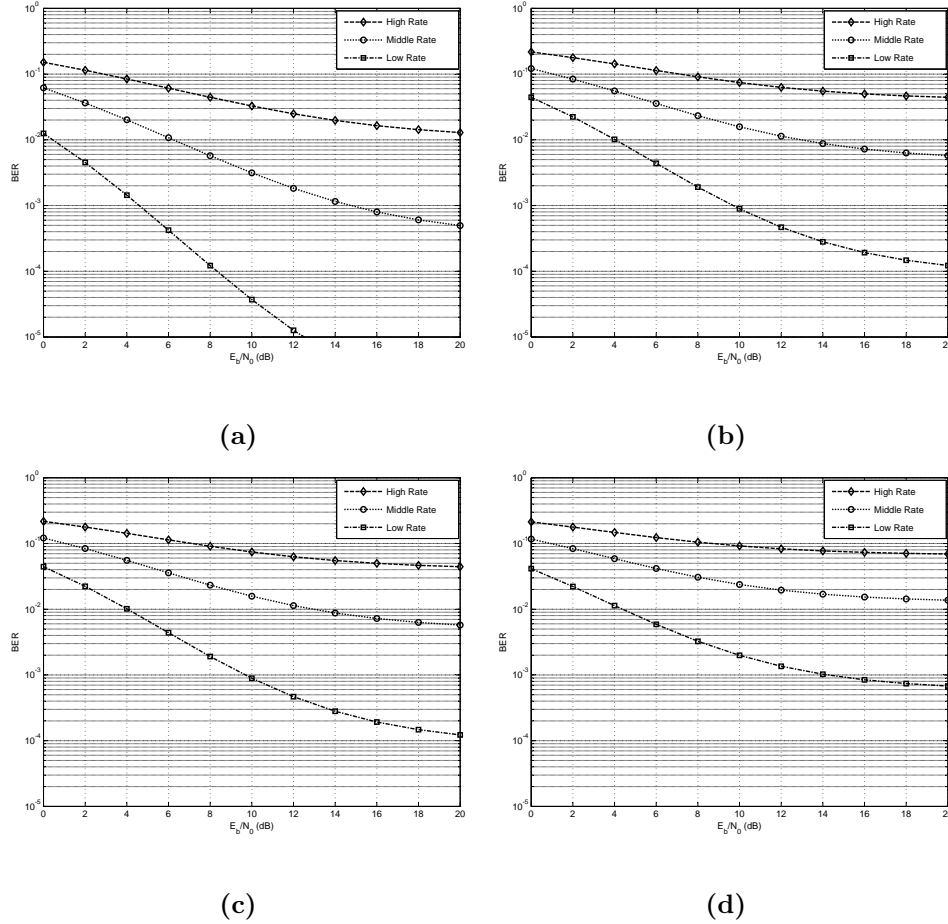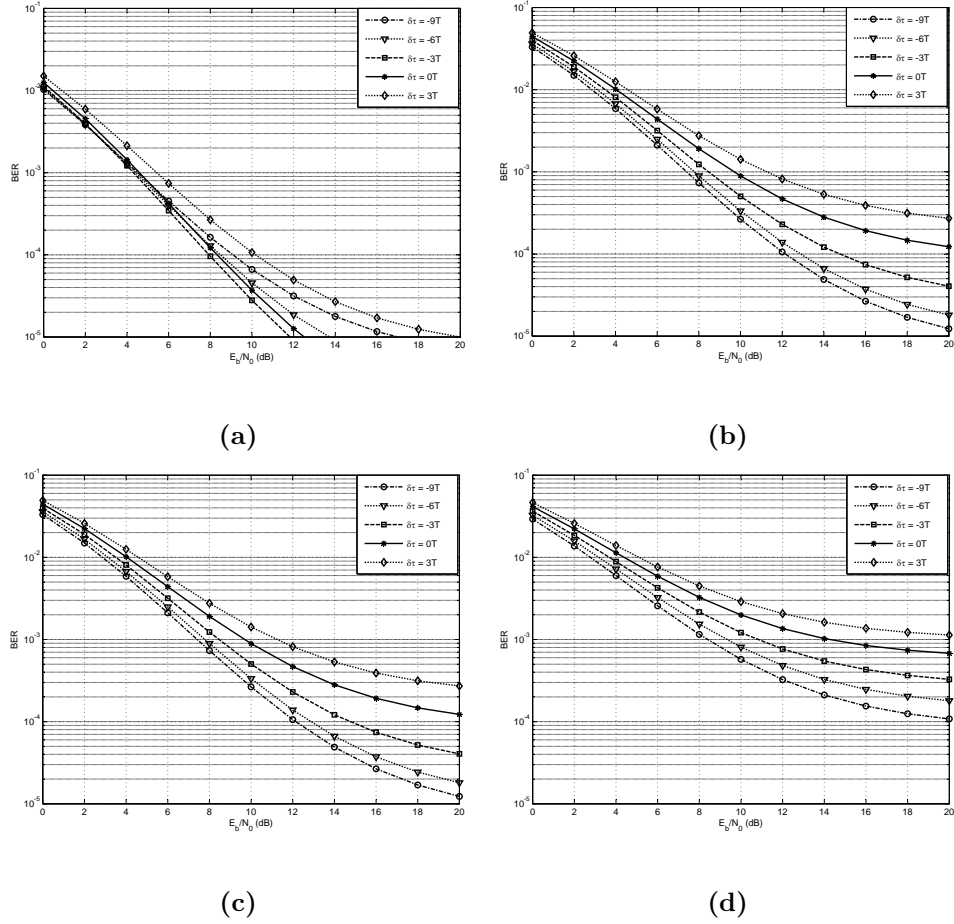
Figure 3.6: **The average probability of bit error of the OFDM system in imperfect timing synchronization in different UWB channel models: (a) CM1; (b) CM2; (c) CM3; and (d) CM4.**

symbol and degrade the system performance. However, since the cyclic prefix region is filled with zeros (called zero trailing), this does not occur. As the absolute value of the negative timing error increases but is still in the cyclic prefix region, its benefit disappears. The performance becomes worse again as shown in Figure 3.6. This is due to the loss of the main components in the arrival signal. As we have known, the energy of the arrival rays and clusters decays exponentially, following Eq. 3.4. Thus the first serval rays in the first cluster have the largest energy and

hold the main role in the recovery of the transmitted symbol. For large but negative timing errors, these rays are shifted far away from their proper positions, causing the performance degradation. As we have seen, the timing synchronization error causes the ISI increment.

The second observation from the figure is that as the channel severity increases, larger negative timing errors are allowed. In Figure 3.6(a), corresponding to CM1, the performance of $\delta\tau = -6T$ where $T = T_S/128$ is already worse than that of $\delta\tau = 0T$ while the performance of $\delta\tau = -9T$ corresponding to CM4 in Figure 3.6(d) is still the best. This is clearly the case since CM4 has the largest channel delay, due to its extreme non-LOS condition and its largest distance between the receiver and transmitter, thus allows the largest negative timing error.

In Figure 3.7, we plot the degradation ratio (dB) between the perfect frequency and timing synchronization and the imperfect frequency synchronization versus the relative carrier-frequency offset ε. The degradation ratio is plotted for the four channel models in different SNR of 0 dB, 10 dB, and 20 dB. Again, two conclusions can be drawn from the figure. First, as the relative carrier-frequency offset increases, the degradation ratio increases, i.e., that the system performance becomes worse since the average SNR $\overline{\gamma_s}(\varepsilon, \tau)$ decreases. The reason is that, in term of energy, the demodulated signal $\hat{c}_{m,i}$ contains less the desired symbol $c_{m,i}$ due to its fading term H_m while contains more the other symbols (the undesired ones), as illustrated in Figure 3.3(b) (when $\varepsilon \neq 0$, the demodulated signal includes not only the desired symbol but also the symbols from other subcarriers). As a result, the imperfect frequency synchronization causes the ICI increment in the demodulated signal and

Figure 3.7: **The degradation ratio of the OFDM system in imperfect frequency synchronization in different UWB channel models. Different signal-to-noise ratios are used 0dB, 10dB, and 20dB: (a) CM1; (b) CM2; (c) CM3; and (d) CM4.**

degrades the system performance.

The second observation is that as the channel severity increases, the degradation ratio decreases. As shown in the figure, the degradation ratio decreases as the SNR decreases, i.e., that the channel is more severe. We also see the similar trend across the channel models. The degradation ratio in CM1 is the largest while it is the smallest in CM4. The reason can be that since the performance is already very bad in the severe channel, the same amount of carrier-frequency offset causes

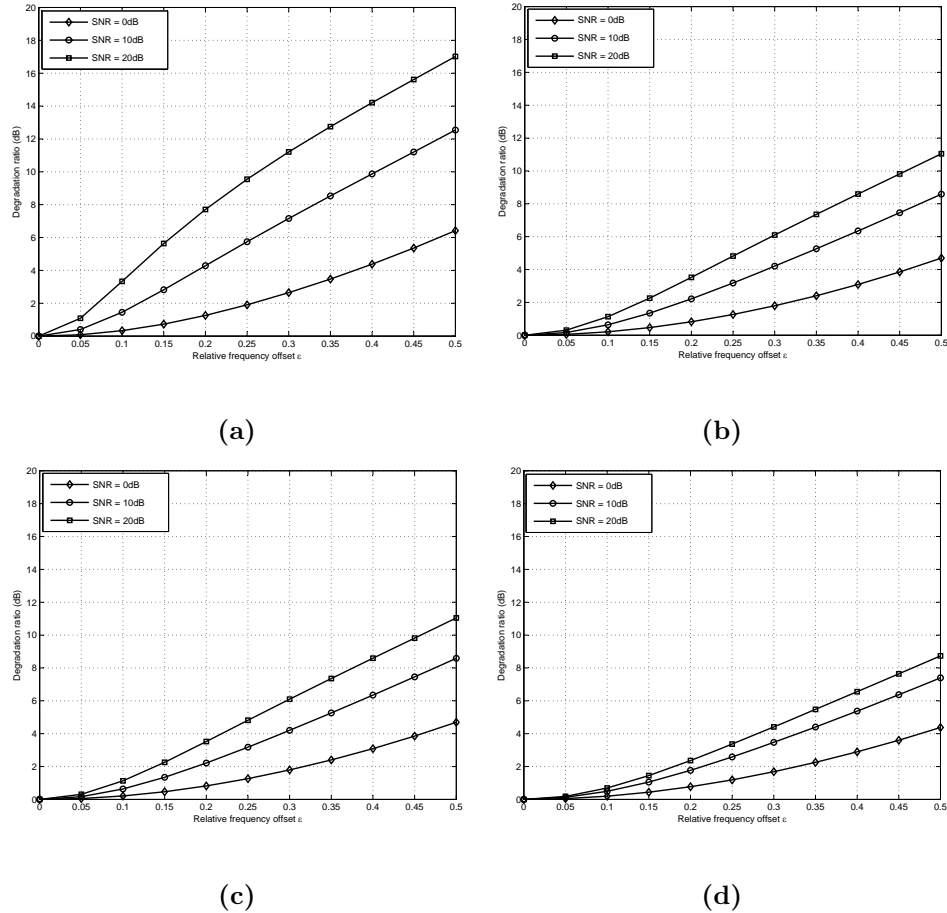a relatively small degradation to the system performance.
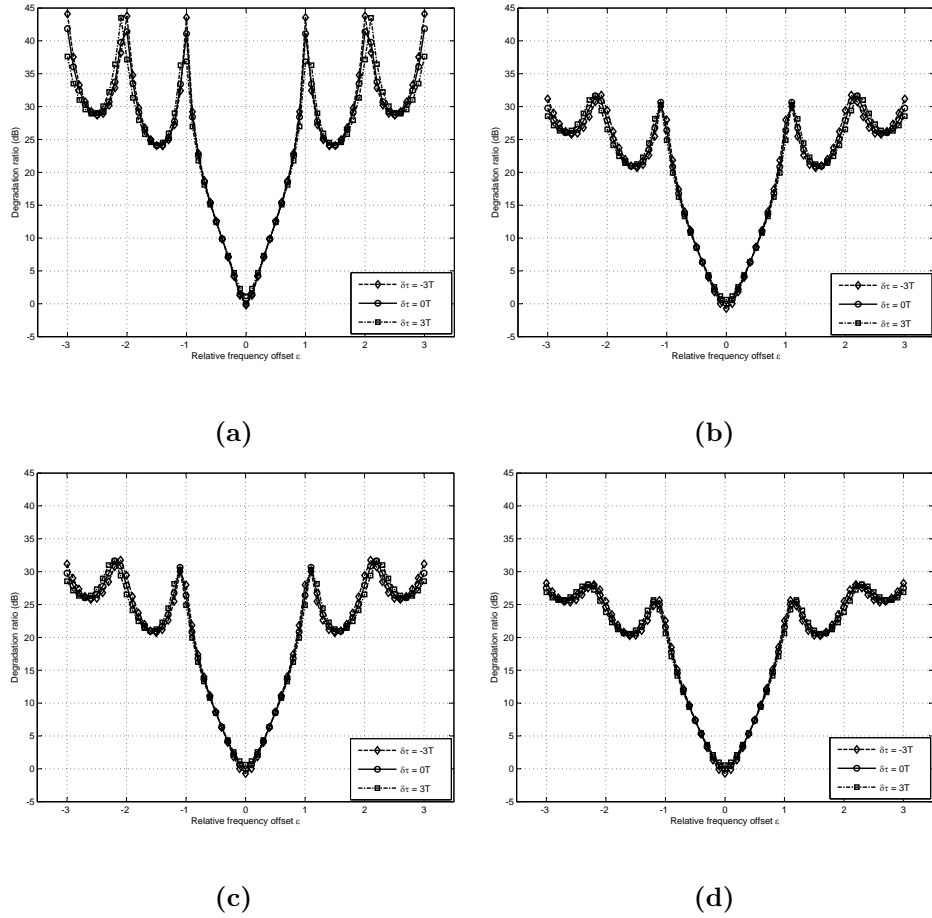
Figure 3.8: **The degradation ratio of the OFDM system in imperfect frequency and timing synchronization in different UWB channel models. The signal-to-noise ratio is 10dB: (a) CM1; (b) CM2; (c) CM3; and (d) CM4.**

The last figure of interest is Figure 3.8, in which we plot the degradation ratio versus the relative carrier-frequency offset ε for various relative timing error $\delta\tau$. The figure reveals that frequency synchronization is more important than timing synchronization. As shown in Figure 3.8(a), the degradation ratio in CM1 is 45 dB when $\varepsilon = \pm 1$ while it is about zero when $\tau = 3$ (and $\varepsilon = 0$). To provide the reason, we will employ Figure 3.3(b) again. The figure illustrates that when ε is a non-zero

integer, the demodulated signal totally loses its transmitted symbol. In this case, it receives a symbol from another subcarrier. Therefore, the degradation ratio should be infinite. However, in our cases, we are still able to receive the desired symbol. The reason is due to the channel multipath delay. This can be seen clearly through Eq. (3.22), which represents the fading term H_m. Without the channel multipath delay, i.e., $T_l = 0$ and $\tau_{k,l} = 0$ and without timing error, i.e., $\tau = 0$, the fading term H_m is identical to zero, and that leads to the loss of the desired symbol.

In the next subsection, we will present the simulated result versus the numerical result.

3.5.2 Simulated vs. Numerical Results

The simulated result is plotted together with the numerical result in Figure 3.9. The vertical axis is the bit error rate (BER), and the horizontal axis is the SNR in dB. So far, we are able to obtain only the simulated average bit error probability for the OFDM system for high-rate mode in the case of channel model CM1 and perfect frequency and timing synchronization. The reason is that the simulation consumes an enormous amount of time. As we have seen, our performance analysis is based on the continuous-time channel impulse response, which consists of high average number of multipath delays. The numbers of delays for CM1, CM2, CM3, and CM4 are 295, 765, 1460, and 3930 in average, respectively. In order to observe the ISI effect, we need to take all multipath delays into account, i.e., to sum them all up. The number of multipath delays together with the number of subcarriers
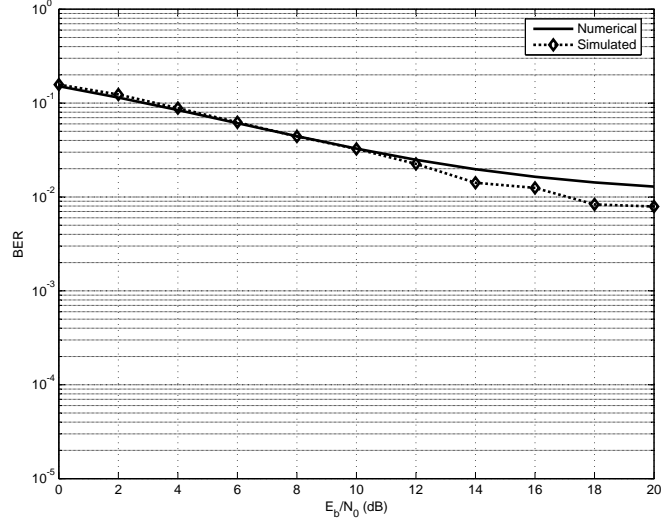
Figure 3.9: **The average bit error probability of the OFDM system for the high data rate mode in channel model CM1.**

($N = 128$) requires a very large number of additions and multiplications for the computation of the received signal $r(t)$, as we see in Eq. (3.8). In addition, the computation of the demodulated signal $\hat{c}_{m,i}$ requires the integration of the received signal $r(t)$, as we see in Eq. (3.12). The definite integral in Eq. (3.12) is performed numerically using methods such as adaptive Simpson's quadrature (MathWorks uses this method in its Matlab built-in function "quad.m"), which require to divide the interval of integration into a number of subintervals, compute the values of the integrand based on the subintervals, sum all the values up, compare with a tolerance (set at 10^{-6}), and repeat the process again with the increasing number of subintervals if the tolerance is not met. For the case in the figure, the integral is evaluated over about 10,000 subintervals. The whole process really consumes a great amount of time in our cases. To obtain one point in Figure 3.9 (the figure consists of 11 points), it takes in average 5 days (120 hrs) with the input of only 1200 bits. For channel

models CM2, CM3, and CM4, computers just cannot handle it.

The accuracy of the simulated result depends on two factors, which eventually target on the number of generated bits in the input sequence. First of all, for a low bit error probability, we need a high number of generated bits. Commonly, for a 10^{-n} bit error rate, where n is a natural number, we need at least 10^{n+1} generated bits to observe such a rate. Secondly, we want to perceive the system average bit error probability, which is an average of the bit error probability for a given channel realization. Since each channel realization convolutes with at least one transmitted symbol, we need to generate a large number of transmitted symbols. Equivalently, we need to generate a large number of bits in the input sequence. For the simulated result, we used only 1200 bits, equivalently to 6 OFDM symbols for the high-rate mode, and thus we could have only 6 channel realizations. However, it took us 5 days as mentioned. To increase the accuracy in our case, we need to generate more OFDM symbols, but that is not possible due to the longer simulation time.

Although we have the difficulty in the simulation due to the limitation of the computing resources, Figure 3.9 shows that the simulated result matches the numerical result very well, at least up to $SNR = 12$ dB. The reason for the mismatch at high SNR is due to the small number of input bits we used in the simulation. The average bit error probability decreases as the SNR increases and thus requires larger number of input bits to realize the decrement. We wish that we have more time and resources to obtain all the desired results. Nevertheless, Figure 3.9 validates our performance analysis.

Chapter 4

Conclusions and Contributions

The work in our thesis includes the baseband implementation and performance analysis of the MB-OFDM UWB system. Since UWB transmission technology is the future technology which promises to fulfill the demand of high transmission data rates, understanding the architecture and the performance of the UWB system is important. The implementation and the performance analysis help us to achieve it.

The baseband implementation of the MB-OFDM UWB system follows the standard proposal IEEE 802.15.3a in a straightforward manner. The baseband system consists of a data scrambler, a convolutional encoder and puncturer, a bit interleaver, a constellation mapper, and an IFFT. These components were completely described in Chapter 2.

We considered the performance analysis of the system in the IEEE 802.15.3a channel standard, which consists of four different channel models, under four different conditions of the frequency and timing synchronization. The MB-OFDM UWB system can be divided into the channel coding and the OFDM subsystems. Our performance analysis was first processed on the OFDM subsystem and after that we considered the performance of the entire system. In the first stage, we first derived the average SNR of the system in the standard channel models. Then we employed degradation ratio and average bit error probability to evaluate the performance of

the OFDM system. Based on the average probability, we presented the way to obtain the performance bound of the entire system. The derivation was completely presented in Chapter 3.

Also in Chapter 3, we presented the numerical results based on the derivation of the system degradation ratio and the average bit error probability. The numerical results provide us a profound understanding of the system performance in the standard channel models under different conditions of the frequency and timing synchronization. Due to the limitation of the computing resources, we could obtain only simulated result of the average bit error probability in the high-rate mode under the channel model CM1. The simulated result matched the corresponding numerical result very well. We wish that we had more time and resources to obtain all the desired results. Nevertheless, the simulated result validated our performance analysis.

Through the implementation and the performance analysis, we have obtained a good understanding about the architecture and the performance of the MB-OFDM UWB system. The understanding would help us improving the system in the future. Since such complete analysis has not been published in the literature, our knowledge about the system performance is the main contribution to the area of wireless communications.

Appendix: C Programming Codes of the Baseband MB-OFDM UWB System

Transmitter:

```c
#include "Transmit_system.h"
#include "readtransmitfile.h"
#include "scramble.h"
#include "convencode.h"
#include"puncture.h"
#include "interleave.h"
#include "constellation.h"
#include "modulation.h"
#include "timespread.h"
#include "writetransmitfile.h"

int main(void)
{
    /*****************************************************************************
     * Here is the main function of the baseband transmit system.               *
     * Transmit System:                                                         *
     *   BitStream --> data_srambler --> convolutional_encoder -->              *
     *   bit_interleaver --> constellation_mapper --> OFDM_modulator -->        *
     *   time_spreader --> TimeSpreadStream                                     *
     *                                                                          *
     * Inputs:                                                                  *
     *   BitStream       : transmit bitstream (the transmit data in binary)     *
     *   Rate            : transmit data rate                                   *
     *                                                                          *
     * Outputs:                                                                 *
     *   TimeSpreadStream    : the transmit baseband signal                     *
     *   Rate               : transmit data rate                               *
     *   NumSymbols       : number of transmit OFDM symbols                     *
     *   SeedID           : two bits seed ID                                    *
     *                                                                          *
     * The output of time_spreader: TimeSpreadStream (which is also the         *
     * output of the baseband transmit system) is fed into the radio            *
     * frequency (RF) system. TimeSpreadStream is transmitted in the frame      *
     * body. Rate, NumSymbols, and SeedID are sent in the physical header.      *
     * For the testing purpose, the values of these variables are stored in     *
     * OutTransmit.out.                                                         *
     *****************************************************************************/

    short   SeedID[2];              /* store seed ID (2 bits)      */
    short   *BitStream;             /* binary bitstream            */
    short   *ConvStream;            /* convolutional encoded stream */
    short   *PuncStream;            /* punctured stream            */
    short   *BitStreamExt;          /* extended bitstream          */
    double  *ConstStream;           /* constellation stream        */
    double  *IfftStream;            /* inverse FFT stream          */
    double  *TimeSpreadStream;      /* time spreading stream       */
```

```
double   DataRate;                        /* transmit data rate              */
int      Rate;                            /* transmit data rate in binary    */
long     Ncbps;                           /* number of coded bit per symbol  */
long     NumSymbols;                      /* number of transmit OFDM symbols */
long     NumSamples;                      /* number of transmit samples      */

printf("\n ******************** TRANSMIT SYSTEM ************************\n\n");

/* Enter the transmit data rate */
printf(" Please enter the transmit data rate.\n");
printf("      Enter 000 for  53.3 Mbps,\n");
printf("      Enter 010 for  55.0 Mbps,\n");
printf("      Enter 001 for  80.0 Mbps,\n");
printf("      Enter 002 for 106.7 Mbps,\n");
printf("      Enter 012 for 110.0 Mbps,\n");
printf("      Enter 003 for 160.0 Mbps,\n");
printf("      Enter 004 for 200.0 Mbps,\n");
printf("      Enter 005 for 320.0 Mbps,\n");
printf("      Enter 006 for 400.0 Mbps,\n");
printf("      Enter 007 for 480.0 Mbps,\n");
printf("      Rate = ");
scanf("\%o", &Rate);

/* Check for valid data rate */
while ((Rate != 000)&&(Rate != 010)&&(Rate != 001)&&(Rate != 002)&&(Rate != 012)
    &&(Rate != 003)&&(Rate != 004)&&(Rate != 005)&&(Rate != 006)&&(Rate != 007)){
    printf("\n Data rate entered is not supportted!!!\n\n");
    printf(" Please reenter the transmit data rate.\n");
    printf("      Enter 000 for  53.3 Mbps,\n");
    printf("      Enter 010 for  55.0 Mbps,\n");
    printf("      Enter 001 for  80.0 Mbps,\n");
    printf("      Enter 002 for 106.7 Mbps,\n");
    printf("      Enter 012 for 110.0 Mbps,\n");
    printf("      Enter 003 for 160.0 Mbps,\n");
    printf("      Enter 004 for 200.0 Mbps,\n");
    printf("      Enter 005 for 320.0 Mbps,\n");
    printf("      Enter 006 for 400.0 Mbps,\n");
    printf("      Enter 007 for 480.0 Mbps,\n");
    printf("      Rate = "); scanf("%o", &Rate);}

/* Convert Rate in binary to DataRate in double */
if (Rate == 000)      DataRate = 53.3;
else if (Rate == 010) DataRate = 55.0;
else if (Rate == 001) DataRate = 80.0;
else if (Rate == 002) DataRate = 106.7;
else if (Rate == 012) DataRate = 110.0;
else if (Rate == 003) DataRate = 160.0;
else if (Rate == 004) DataRate = 200.0;
else if (Rate == 005) DataRate = 320.0;
else if (Rate == 006) DataRate = 400.0;
else if (Rate == 007) DataRate = 480.0;

/* Determine Ncbps */
if (DataRate <= 80.0)
```

```
        Ncbps = 100;
    else
        Ncbps = 200;


    /* Read a binary bitstream from input_bitstream */
    printf("\n Reading a binary bitstream...\n\n");
    BitStream = read_file(&NumSamples);


    /* Apply data scrambling and returning seed id */
    printf(" Data scrambling ...\n\n");
    data_srambler(BitStream, SeedID, NumSamples);


    /* Apply convolutional encoding with coding rate 1/3 */
    printf(" Convolutional encoding ...\n\n");
    ConvStream = conv_encoder(BitStream, &NumSamples);
    free(BitStream);


    /* Apply punctring to obtain different coding rates */
    printf(" Puncturing ...\n\n");
    PuncStream = puncturer(ConvStream, &NumSamples, DataRate);
    free(ConvStream);


    /* Apply bit-interleaving */
    printf(" Bit interleaving ...\n\n");
    BitStreamExt = bit_interleaver(PuncStream, &NumSamples, Ncbps);
    free(PuncStream);


    /* Apply subcarrier constellation mapping */
    printf(" Constellation mapping ...\n\n");
    ConstStream = const_mapper(BitStreamExt, NumSamples);
    free(BitStreamExt);


    /* Apply OFDM_modulation */
    printf(" OFDM modulation ...\n\n");
    IfftStream = OFDM_modulation(ConstStream, DataRate, Ncbps, ...
                                 NumSamples, &NumSymbols);
    free(ConstStream);


    /* Apply time spreading */ printf(" Time spreading ...\n\n");
    TimeSpreadStream = time_spreader(IfftStream, DataRate, &NumSymbols);
    free(IfftStream);


    /* Write to a transmit file */
    printf(" Writing to OutTransmit.out ...\n\n");
    write_file(Rate, NumSymbols, SeedID, TimeSpreadStream);
    free(TimeSpreadStream);


    return 0;
}
```

Receiver:

```
#include "Receive_system.h"
#include "readreceivefile.h"
#include "demodulation.h"
#include "deinterleave.h"
#include "depuncture.h"
#include "Viterbidecode.h"
#include "descramble.h"
#include "writereceivefile.h"

int main(void) {
    /*****************************************************************************
    * Here is the main function of the baseband receive system.               *
    *                                                                         *
    * Receive system:                                                         *
    *   TimeSpreadStream --> OFDM_demodulator --> bit_deinterleaver -->       *
    *   Viterbi_decoder --> data_desrambler --> ReBitstream                   *
    *                                                                         *
    * Inputs:                                                                 *
    *   TimeSpreadStream: the received baseband signal from frame payload     *
    *   Rate            : transmit data rate                                  *
    *   NumSymb         : number of transmit OFDM symbols                     *
    *   SeedID          : two bits seed ID                                    *
    *                                                                         *
    * Output:                                                                 *
    *   ReBitStream     : the reconstructed bitstream                         *
    *                                                                         *
    * TimeSpreadStream is fed from the radio frequency (RF). Rate, NumSymb,   *
    * and SeedID are from the physical header.  For the testing purpose,      *
    * the values of these variables are read from OutTransmit.out.            *
    * ReBitstream is stored in ReBitstream.out.                               *
    *****************************************************************************/

    short   SeedID[2];                  /* store seed ID (2 bits)         */
    double  *TimeSpreadStream;          /* time spreading stream          */
    short   *DeStream;                  /* demodulation stream            */
    short   *DePuncStream;              /* depunctured stream             */
    short   *ReBitStream;               /* received bitstream             */
    long    NumSamp;                    /* number of samples              */
    long    Ncbps;                      /* number of coded bit per symbol */
    long    NumSymb;                    /* number of OFDM symbols         */
    double  DataRate;                   /* transmit data rate             */
    int     Rate;                       /* transmit data rate in binary   */

    printf("\n ********************** RECEIVE SYSTEM **********************\n\n");

    /* Read receives signal from OutTransmit.out */
    printf(" Read received signal ...\n\n");
    TimeSpreadStream = read_file(&Rate, &NumSymb, SeedID);

    /* Convert Rate in binary to DataRate in double */
    if (Rate == 000)      DataRate = 53.3;
    else if (Rate == 010) DataRate = 55.0;
```

```
        else if (Rate == 001) DataRate = 80.0;
        else if (Rate == 002) DataRate = 106.7;
        else if (Rate == 012) DataRate = 110.0;
        else if (Rate == 003) DataRate = 160.0;
        else if (Rate == 004) DataRate = 200.0;
        else if (Rate == 005) DataRate = 320.0;
        else if (Rate == 006) DataRate = 400.0;
        else if (Rate == 007) DataRate = 480.0;


        /* Apply OFDM de-modulation */
        printf(" OFDM de-modulation ...\n\n");
        DeStream = OFDM_de_modulation(TimeSpreadStream, &NumSamp, &Ncbps, ...
                                     DataRate, NumSymb);
        free(TimeSpreadStream);


        /* Apply bit deinterleaving */
        printf(" Bit de-interleaving ...\n\n");
        inv_bit_interleaver(DeStream, NumSamp, Ncbps);


        /* Apply inverse puncturing */
        printf(" Inverse puncturing ...\n\n");
        DePuncStream = inv_puncturer(DeStream, &NumSamp, DataRate);
        free(DeStream);


        /* Apply Viterbi decoding */
        printf(" Viterbi decoding ...\n\n");
        ReBitStream = viterbi_decoder(DePuncStream, &NumSamp);
        free(DePuncStream);


        /* Apply inverse data scrambling */
        printf(" Inverse data scrambling ...\n\n");
        inv_data_srambler(ReBitStream, SeedID, NumSamp);


        /* Write the ReBitStream into ReBitStream.out */
        write_file(ReBitStream, NumSamp);
        free(ReBitStream);
        return 0;
}
```

BIBLIOGRAPHY

[1] FCC02-48, "Revision of part 15 of the commission's rules regarding ultra wide-band transmission systems, first report and order." `http://www.fcc.gov/Bureaus/Engineering_Technology/Orders/2002/fcc02048.pdf`.

[2] F. Adachi, "Broadband mobile technology." Internet. `http://www.atis.org/tg2k/`.

[3] K. Santhi *et al.*, "Goals of true broad band's wireless next wave (4G-5G)," *IEEE VTC'03*, vol. 4, pp. 2317–2321, Oct. 2003.

[4] S. Huang, "Evolution from 3G to 4G and beyond (5G)." Internet. `http://www.daniweb.com/techtalkforums/thread35959.html`.

[5] D. Porcino and W. Hirt, "Ultra-wideband radio technology: Potential and challenges ahead," *IEEE Communications Magazine*, vol. 41, pp. 66–77, July 2003.

[6] T. M. Cover and J. A. Thomas, *Elements of Infomation Theory*. New York, USA: John Wiley and Sons, 1991.

[7] R. Fisher *et al.*, "DS-UWB physical layer submission to 802.15 task group 3a," tech. rep., IEEE P802.15-04/0137r3, July 2004.

[8] A. Batra *et al.*, "Multi-band OFDM physical layer proposal for IEEE 802.15 task group 3a," tech. rep., IEEE P802.15-03/268r3, March 2004.

[9] "IEEE 802.15: Working group for wireless personal area networks (WPANs)." Internet. `http://www.ieee802.org/15/`.

[10] J. Foerster *et al.*, "Channel modeling sub-committer report final," tech. rep., IEEE P802.15-02/368r5-SG3a, July 2004.

[11] Y. Park *et al.*, "Performance of UWB DS-CDMA/OFDM/MC-CDMA system," *MWSCAS'04*, vol. 1, pp. I–37–40, July 2004.

[12] O. Shin *et al.*, "Performance evaluation of MB-OFDM and DS-UWB systems for wireless personal area networks," *IEEE ICUWB'05*, pp. 214–219, September 2005.

[13] C. Snow *et al.*, "Performance analysis of multiband OFDM for UWB communication," *IEEE ICC'05*, vol. 4, pp. 2573–2578, May 2005.

[14] W. P. Siriwongpairat, W. Su, and K. J. R. Liu, "Characterizing performance of multiband UWB systems using Poisson cluster arriving fading paths," *6th IEEE Workshop on Signal Processing Advances in Wireless Communications*, pp. 246–250, 2005.

[15] ATIS, "Atis telecom glossary 2000." Internet. `http://www.atis.org/tg2k/`.

[16] C. Fleming, "A tutorial on convolutional coding with viterbi decoding." Internet. `http://home.netcom.com/~chip.f/Viterbi.html`.

[17] "Wikipedia - the free encyclopedia." Internet. `http://en.wikipedia.org/wiki/Main_Page`.

[18] A. Leon-Garcia, *Probability and Random Processes for Electrical Engineering.* USA: Addison Wesley Longman, 2nd ed., 1994.

[19] W. P. Siriwongpairat, W. Su, and K. J. R. Liu, "Performance characterization of multiband UWB communication systems using Poisson cluster arriving fading paths," *IEEE ...*, vol. B313, pp. 458–460, 1993.

[20] J. R. Barry, E. A. Lee, and D. G. Messerschmitt, *Digital Communication.* USA: Kluwer Academic Publishers, 3rd ed., 2004.

[21] J. G. Proakis, *Digital Communications.* NewYork, USA: McGraw-Hill, 4th ed., 2001.

[22] R. A. Horn and C. R. Johnson, *Matrix Analysis.* New York, USA: Cambridge University Press, 1985.

[23] A. M. Mathai and S. B. Provost, *Quadratic Forms in Random Variables: Theory and Applications.* New York, USA: Marcel Dekker Inc., 1992.

[24] M. K. Simon and M. S. Alouini, *Digital Communication over Fading Channels: A Unified Approach to Performance Analysis.* New York, USA: John Wiley and Sons, 2000.

[25] J. Hagenauer, "Rate-compatible punctured convolutional codes (RCPC codes) and their applications," *IEEE Transactions on Communications*, vol. 36, pp. 389–400, April 1988.